

Title	Sedimentary features observed in the tsunami deposits at Rikuzentakata City
Author(s)	Naruse, Hajime; Arai, Kazuno; Matsumoto, Dan; Takahashi, Hiroki; Yamashita, Shota; Tanaka, Gengo; Murayama, Masafumi
Citation	Sedimentary Geology (2012), 282: 199-215
Issue Date	2012-12
URL	http://hdl.handle.net/2433/166602
Right	© 2012 Elsevier B.V.
Type	Journal Article
Textversion	author

1 Sedimentary features observed in the tsunami deposits at Rikuzentakata City

Hajime Naruse^{1*}, Kazuno Arai², Dan Matsumoto³, Hiroki Takahashi², Shota Yamashita², Gengo Tanaka⁴, and Masafumi Murayama⁵

¹Kyoto University, Division of Earth and Planetary Sciences, Graduate School of Science, Kitashirakawa-Oiwakecho, Sakyo-ku, Kyoto 606-8502, Japan

²Chiba University, Division of Earth Sciences, Graduate School of Science, 1-33 Yayoicho, Inage-ku, Chiba 263-8522, Japan

³Advanced Industrial Science and Technology, Institute of Geology and Geoinformation, 1-1-1 Higashi, Tsukuba, Ibaraki 305-8561, Japan

⁴Gunma Museum of Natural History, 1674-1, Kamikuroiwa, Tomioka-shi, Gunma 370-2345, Japan

⁵Kochi University, Center for Advanced Marine Core Research, B200 Monobe, Nankoku, Kochi 783-8502, Japan

*Corresponding author: naruse@kueps.kyoto-u.ac.jp Fax: +81-75-753-4189

Abstract

4 The March 11, 2011 Tohoku-Oki tsunami triggered by an earthquake off the
5 east coast of northeastern Honshu Island (Tohoku region), Japan, deposited large
6 amounts of sediment on land, including the Sendai Plain and Sanriku Coast. This study
7 reports on the characteristics of the tsunami deposits in Rikuzentakata City, southeastern
8 Iwate Prefecture, northeastern Japan. A field survey identified the inundation pattern of
9 the tsunami in this region and the facies model of the tsunami deposits at the bay-head
10 deltas of estuarine systems. The tsunami deposits in Rikuzentakata City generally
11 consist of one to four units that represent a discrete runup or backwash flow. Each unit
12 is characterized by initial inverse grading and successive normal grading that
13 correspond to the accelerating and decelerating stages of the flow, respectively. An
14 internal erosional surface often developed between the inverse-graded and
15 normal-graded units. It corresponds to the maximum shear velocity of the flow and
16 truncates the underlying inverse-graded unit. In the case of the runup unit, silty
17 fine-grained drapes overlay the graded sandy interval. A correlation of the sedimentary
18 structures and grain fabric analysis revealed that the Tohoku-Oki tsunami inundated
19 Rikuzentakata City at least twice and that the flow velocity exceeded 2.4 m/s.
20 Paleontological analysis of the sediment and kriging estimation of the total volume of
21 the tsunami deposit implied that the sediments were sourced not only from eroded beach
22 sands but also from the seafloor of Hirota Bay or more offshore regions.

23 KEYWORDS: tsunami; inverse-graded bedding; graded bedding; Northwest Pacific;

24 ostracods

25

26 1. Introduction

27 The Tohoku-Oki tsunami was triggered by an earthquake that occurred at 14:46
28 on March 11, 2011, with the epicenter located off the east coast of northeastern Honshu
29 Island (Tohoku region), Japan (Fig. 1). The Mw 9.0 earthquake is the largest recorded
30 event in Japan (Fujii et al., 2011) and the fourth-largest in the last 100 years in the
31 World (Nettles et al., 2011). According to the Japan Meteorological Agency, the
32 earthquake resulted from a series of seismogenic faulting events that began at
33 38.1035°N, 142.861°E, Mw 9.0 at 14:46:18 JST, along the Japan Trench, where the
34 Pacific Plate is subducting beneath the North American Plate. The resulting tsunami
35 spread across the North Pacific Ocean (Stimpson, 2011), striking coastal areas of Japan
36 with a maximum run-up height of 39.7 m in Miyako city, Japan (Mori et al., 2011). As
37 of 8 August, 2012 (National Policy Agency of Japan, 2012), the estimated fatalities
38 were 15,868 with 2,848 persons still missing.

39 The tsunami inundation caused severe damage, especially in the coastal regions
40 of northeastern Japan, such as Fukushima, Miyagi, and Iwate Prefectures. This study
41 reports on the characteristic features of the tsunami deposits in Rikuzentakata City,
42 southeastern Iwate Prefecture, northeastern Japan (Figs. 1 and 2). The city suffered
43 catastrophic destruction (Figs. 3 and 4) with an estimated 1,552 fatalities and an
44 additional 399 persons missing as of July 14, 2011
45 (<http://sv032.office.pref.iwate.jp/~bousai/>). This is the largest number of fatalities in
46 Iwate Prefecture. The city remains at risk from future tsunamis, as do other areas with
47 similar topographic features, thus it is important to understand the behavior of tsunami

48 waves in this region for future disaster mitigation. Another significance of the research
49 in this region is that a field survey in Rikuzentakata City may potentially reveal features
50 of tsunami deposition in natural environments without the influence of artificial
51 infrastructure. Most cities on the Sanriku Coast were protected by artificial coastal
52 levees, aiming at trapping most of the sediment transported by tsunami waves. Hence,
53 less deposition is expected than in the case of ancient tsunami deposits. In the case of
54 Rikuzentakata City, however, the first tsunami wave completely destroyed a 5.5-m-high
55 coastal levee, resulting in large-scale erosion of the sandy coast (Fig. 3). This coastal
56 erosion provided abundant source sediments that were deposited on land, forming a
57 thick and extensive tsunami deposit. Therefore, it is expected that the facies model of
58 the tsunami deposits in this region may be comparable to ancient events and will be
59 helpful in deciphering geological records. There are also extensive studies of the 2011
60 Tohoku-Oki tsunami deposits on the Sendai Plain (e.g. Goto et al., 2011; submitted this
61 issue; Abe et al., in press this issue), and therefore the future comparison of results
62 between the Sanriku Coast and Sendai Plain regions will be significant, focusing on
63 influences of topographic settings on the sedimentary features of tsunami deposits.

64 This study aims to contribute to future research on tsunami deposits and
65 disaster prevention from two viewpoints: (1) providing information about the behavior
66 of the Tohoku-Oki tsunami in this region and (2) establishing a facies model of the
67 tsunami deposits at the bay-head deltas of estuarine systems. Terrestrial tsunami
68 deposits provide important information on the magnitude and recurrence intervals of
69 tsunami events (Nanayama et al., 2003). Reconstruction of the hydraulic properties and
70 magnitude of historical tsunamis from stratigraphic sequences can be useful in risk
71 assessment studies. However, sandy beds in coastal stratigraphic successions may also

72 be produced by events such as large-scale storms and river flooding (e.g., Switzer &
73 Jones, 2008). Therefore, it is important to investigate the detailed features of recent
74 tsunami deposits from known source events because their sedimentological
75 characterization and relationship with the actual events are necessary for establishing
76 the criteria to identify tsunami deposits in the geological record.

77 Documentation of the Tohoku-Oki tsunami is also significant for the
78 verification and improvement of numerical tsunami models, which will be important for
79 future disaster-prevention measures. Direct measurements of flow velocities or
80 hydrographs of the tsunami are not available for this region; hence, an investigation of
81 the deposits is useful in providing information on this hazard. From this viewpoint, the
82 study examined the number of inundations, estimated minimum flow velocities, and
83 calculated the total flux of tsunami sediment. These characteristics will be reproduced in
84 future studies by numerical models with sediment transport functions.

85 2. Study Region

86 Rikuzentakata City, on the southern Sanriku Coast, is approximately 130 km
87 west of the earthquake epicenter (Fig. 1). The central–southern part of the Sanriku Coast
88 is a mountainous region with a deeply indented Ria coastline, which features a series of
89 alternating capes and estuaries, with small bay-head deltas often developed at the river
90 mouths.

91 Rikuzentakata City is located in an estuarine bay-head delta plain in the inner
92 part of Hirota Bay (Fig. 1 and 2). The coastal delta plain is approximately 2 km wide in
93 the north–south direction and extends for 2.5 km east–west. Most regions of the

94 delta-plain are relatively flat and are less than 5 m above mean sea level. This delta
95 plain was formed by the 50 km long Kesen River, which has a drainage basin area of
96 540 km². Progradation of the delta was initiated approximately 6000 years before
97 present in response to Holocene sea level rise, and the modern delta plain was mostly
98 established by about 3000 years before present (Chida et al., 1984). The most prominent
99 topographic feature of Rikuzentakata City was the Takata-Matsubara pine forest, located
100 on a wave-dominated spit (Fig. 3) on top of which a 5.5-m-high coastal levee had been
101 built (Asano et al., 2009).

102 The maximum tsunami run-up height was 19.9 m in this region, and the
103 inundation height (tsunami height above mean sea level) was approximately 14–15 m
104 (reported by The 2011 Tohoku Earthquake Tsunami Joint Survey Group at
105 <http://www.coastal.jp/tjt/>). The exact number of inundations and periodicity of the
106 tsunami waves at Rikuzentakata City is unknown because all tidal gauges and global
107 positioning system (GPS) buoys in this area were destroyed by the event. However, data
108 from a GPS buoy located off southern Iwate Prefecture (39.3361°N, 141.9944°E), ca. 15
109 km offshore, indicate that seven successive waves struck this coast (Takahashi et al.,
110 2011). The first wave was the largest (6.7 m in height at this site), the second and fourth
111 waves were relatively high (approximately 2 m in height), and others were relatively
112 small (less than 1.5 m in height). The wave periodicity was approximately 50 min
113 (Takahashi et al., 2011). Numerical simulation suggests that the tsunami showed a
114 similar wave pattern close to Rikuzentakata City (Fujii et al., 2011). However, the
115 complicated shape of the Sanriku coastline influences wave height and periodicity near
116 the coast and so tsunami waves inundating the coast cannot be expected to precisely
117 follow the patterns indicated by these offshore data.

118 The 2011 Tohoku-Oki tsunami largely eroded the spit in this region,
119 transporting a large amount of sandy sediments on land. Takata-Matsubara was
120 artificially designed to prevent storm and tsunami disasters, and had previously resisted
121 two major tsunamis, the 1896 Meiji Sanriku Tsunami and the 1933 Showa Sanriku
122 Tsunami (Asano et al., 2009). However, the forest was completely destroyed by the
123 2011 Tohoku-Oki tsunami and only one pine tree survived, indicating the intensity of
124 the event. Tsunami waves easily spilled over and destroyed the levee behind
125 Takata-Matsubara (Figs. 3 and 4). As a result, most of the city was inundated to a
126 distance of more than 2 km from the shoreline, covering an area of 13 km² from the map
127 provided by Geospatial Information Authority of Japan and the analysis by the Tsunami
128 Damage Mapping Team, Association of Japanese Geographers
129 (http://danso.env.nagoya-u.ac.jp/20110311/map/index_e.html; Fig. 2).

130 3. Methodology

131 We surveyed the topographic features (erosional structures and bedforms) of
132 tsunami inundation and investigated sedimentary features of the tsunami deposits by
133 visual observation, grain-size and fabric analysis. Micropaleontological analysis was
134 also conducted to help estimate sediment sources.

135 3.1 Field Survey

136 We conducted approximately one week of fieldwork in Rikuzentakata City
137 between April 24–26 and June 10–12, 2011. The inundated region of Rikuzentakata
138 City can be subdivided into the main city and the Otomo area, a small settlement a few

139 km from the main town and located on flat land at the end of Hirota Peninsula (Fig. 2).
140 Our survey covered both inundated regions, mostly focusing on areas that were
141 originally rice fields. While buildings and artificial structures have complex effects on
142 tsunami waves, the rice fields are flat and are therefore expected to display the primary
143 features of tsunami deposition without artificial influences. The alignment of felled
144 power poles and crests of bedforms (dunes) were measured to estimate the flow
145 directions of tsunami waves (Fig. 4 and 5).

146 Study site locations were established using a GPS. For each observation site,
147 we examined the erosional features and the distribution of tsunami sediments and
148 excavated pits to measure the sediment thickness and depositional structures.

149 Bulk sediment samples for grain-size and micropaleontological analysis were
150 also taken from each sampling pit. At several locations where the tsunami deposits were
151 relatively thick (~10 cm), trenches several meters long and 10 to 40 cm deep were
152 excavated, and the trench walls were peeled off onto cloth by using polyurethane resin
153 (Fig. 6), in order to examine details of the sedimentary structures and conduct
154 grain-fabric analysis.

155 3.2 Grain-size Analysis

156 Grain-size distributions of tsunami deposits were analyzed using a Mastersizer
157 2000 laser granulometer (Malvern Instruments, Malvern, UK). Before analysis, the
158 organic matter was removed using hydrogen peroxide, and sieving was performed to
159 separate sediments coarser than 2 mm. Samples were then treated with sodium
160 hexametaphosphate as dispersant to scatter the fine sediments (Sperazza et al., 2004).
161 We converted the measured grain sizes to the phi scale ($\phi = -\log_2 D$ where D is the

162 particle diameter in mm). Mean grain size $\bar{\phi}$, sorting s , skewness S_k , and kurtosis
 163 K_t were calculated on the basis of the moment method (Folk, 1966; Harrington, 1967),
 164 as follows:

$$165 \quad \bar{\phi} = \frac{\sum p\phi_i}{100} \quad (1)$$

$$166 \quad s = \sqrt{\frac{\sum p(\phi_i - \bar{\phi})^2}{100}} \quad (2)$$

$$167 \quad S_k = \frac{\sum p(\phi_i - \bar{\phi})^3}{100s^3} \quad (3)$$

$$168 \quad K_t = \frac{\sum p(\phi_i - \bar{\phi})^4}{100s^4} \quad (4)$$

169 where ϕ_i is a representative value of each grain-size class (every 0.17 phi), and p is
 170 a weight fraction (in percentage) for each grain-size class. The 10th, 50th, and 90th
 171 percentile grain-size values D_{10} , D_{50} and D_{90} respectively, were also provided for
 172 each sample.

173 We measured gravels directly with a caliper and described the length of their
 174 b-axes as a representative diameter for the computation of the critical flow velocity,
 175 which is described in section 3.3.

176 3.3 Critical Flow Velocity of Particle Motion

177 The minimum estimation of the flow velocity of the tsunami wave was derived
 178 from grain-size analysis and the size of the largest particles (>2 mm in b-axis diameter)
 179 on the basis of the critical shear stress of initiation of particle motion with consideration
 180 of mixed grain-size effect. Here, the hydraulics of oscillatory flows caused by the waves
 181 are approximated by using uni-directional open-channel flows because the periodicity of
 182 tsunami waves is sufficiently long to justify this approximation. Indeed, the GPS buoy

183 measurement suggested that the periodicity of the Tohoku-Oki tsunami near
 184 Rikuzentakata City was approximately 50 min (Takahashi et al., 2011). Therefore,
 185 critical Shields values τ_c^* can be regarded as those commonly used to denote
 186 conditions under which bed sediment particles are stable but on the verge of being
 187 entrained in open-channel flows. A fit to the Shields data by Brownlie (1981) with
 188 modification proposed by Neil and Yalin (1969) is as follows (Garcia, 2008):

$$189 \quad \tau_c^* = 0.11Re_p^{-0.6} + 0.03\exp(-17.77Re_p^{-0.6}) \quad (5)$$

190 where Re_p is the particle Reynolds number, defined as $Re_p = \sqrt{RgD}D/\nu$ (R :
 191 submerged specific density of sediments (1.65), g : acceleration due to gravity (9.81
 192 m/s²), D : sediment diameter, and ν : kinematic viscosity of ambient fluid), and where
 193 the dimensionless Shields shear stress is defined as follows:

$$194 \quad \tau^* = \frac{u_*^2}{RgD} \quad (6)$$

195 Here, u_* denotes shear velocity. Thus, the critical Shields shear stress τ_{c50}^* for
 196 particles of median grain-size D_{50} can be calculated by equation 5. However,
 197 mixed-size grains do not act the same as when they are surrounded by grains of the
 198 same size (Einstein, 1950), and the coarser grains exposed on the surface protrude more
 199 into the flow, resulting in a preferentially greater drag. This exposure effect (hiding
 200 effect) can be corrected by considering a power-law relationship:

$$201 \quad \frac{\tau_{ci}^*}{\tau_{c50}^*} = \left(\frac{D_i}{D_{50}} \right)^{-\gamma} \quad (7)$$

202 where γ is an empirical parameter that varies from 0.0 to 1.0 (Parker, 2005). From
 203 equations 6 and 7, the critical depth-averaged flow velocity $U_{c\max}$ of the largest grain

204 (diameter is D_{\max}) in the tsunami deposit can be calculated from the following
 205 equation:

$$206 \quad U_{c \max} = C_f^{-\frac{1}{2}} \sqrt{RgD_{\max} \left(\frac{D_{\max}}{D_{50}} \right)^{-\gamma} \tau_{c50}^*} \quad (8)$$

207 Here, C_f is a friction coefficient of uni-directional open-channel flows, defined as
 208 follows:

$$209 \quad U_{c \max} = C_f^{-\frac{1}{2}} u_{*c \max} \quad (9)$$

210 To estimate the critical flow velocity of initiation of particle motion, two
 211 empirical parameters, γ and C_f , must be determined. The value of γ generally
 212 ranges from 0.65 to 0.90 (Parker, 2005), and becomes zero in the case of very large
 213 grains (Ramette and Heuzel, 1962); hence, we considered the value zero when
 214 estimating the flow velocity of the tsunami wave from the largest grain in the deposit.
 215 On the other hand, for hydraulically rough flows, the friction coefficient C_f is given
 216 by the following equation:

$$217 \quad C_f = \left[\frac{1}{\kappa} \ln \left(11 \frac{H}{k_s} \right) \right]^{-2} \quad (10)$$

218 where κ is the Karman constant (~ 0.4); H , the flow thickness; and k_s , the effective
 219 roughness height (Keulegan, 1938). k_s is empirically considered to be proportional to
 220 a representative sediment size D_{90} , such that the following relationship holds:

$$221 \quad k_s = \alpha D_{90} \quad (11)$$

222 The suggested value of α is 3.0 (Van Rijn, 1982). It is difficult to precisely estimate
 223 the flow height of the tsunami wave during deposition of the bed in which the particles
 224 of the maximum grain-size occurred, so we tentatively set the flow height as 10–15 m.

225 The critical flow velocity required to transport the maximum grain-size
226 observed at each site can be estimated using equations 5, 8, 10, and 11. The estimated
227 velocity is, however, the minimum requirement for the tsunami waves that hit
228 Rikuzentakata City. As suggested by Hiscott (1994), the actual flow velocity could far
229 exceed the critical flow velocity of particle motion.

230 3.4 Grain Fabric Analysis

231 The grain fabric of vertical sections of sandy tsunami deposits was examined to
232 analyze the paleocurrent of the oscillatory flows. Trenches were excavated at several
233 localities parallel to the direction of the paleoflow which was estimated by the bedform,
234 and a peel of the trench wall was obtained using polyurethane resin and a mesh.
235 High-resolution images of the peeled sample were captured using a digital camera at
236 4800 dpi. All the grains identified in the images were traced manually, and then each
237 traced grain was approximated by an ellipse, using the public-domain ImageJ program
238 (<http://rsb.info.nih.gov/ij/>). The locations and elongation directions of the grains were
239 obtained as quantitative image-analysis data. The location was taken as the average of the
240 x and y coordinates of pixels included in the traced grain, and the elongation direction
241 was obtained as the angle between the primary axis of an ellipse fitted to the grain by the
242 Hough transform and the line parallel to the x axis of the image. All measured data are
243 considered to be the apparent two-dimensional characteristics of three-dimensional
244 features. The present study therefore examines only the apparent features of the tsunami
245 deposit samples, assuming equivalence to the three-dimensional structure.

246 3.5 Micropaleontology

247 In order to determine the sediment source, we investigated ostracods included
248 in the onshore tsunami deposits formed by the Tohoku-Oki tsunami. Ostracods are small
249 crustacea (0.3–30 mm long) with calcified valves adapted to practically every aquatic
250 environment. Thus, fossilized valves are an important paleoenvironmental indicator,
251 particularly with regard to Holocene oceanographic, climatologic, and geologic events
252 (Nelson et al., 2008). Marine podocopid ostracods are exclusively benthic crustaceans
253 that are abundant in marine sediments. Furthermore, most species show regional
254 endemism, and hence, they can be an important indicator of local bottom-water
255 environments. The valves behave like sediment grains in the water column. We
256 collected ostracod specimens by sieving and manual picking, and then used the modern
257 analog technique (MAT) to infer paleoenvironmental conditions by comparing fossil
258 ostracod assemblages in the onshore sediments with similar assemblages in the modern
259 environment (Ikeya and Cronin, 1993). We compared Holocene ostracod assemblages
260 sampled from 476 surface sediments of the seafloor around Japan with those recovered
261 from sediments deposited by the tsunami, approximately 4 km southeast of
262 Rikuzentakata City (Fig. 2).

263 3.6 Spatial Interpolation of Measured Data

264 The kriging method was employed to estimate the spatial variations in mean
265 grain-size and thickness parameters (Burgess and Webster, 1980a,b; Kohsaka, 1998).
266 Kriging is an algorithm based on least-squares and is used to estimate the spatial
267 variation in a real-valued function; it is based on the assumption that the spatial
268 variation can be estimated from a linear combination of measured values (Kohsaka,

269 1998). Weighting coefficients are obtained on the basis of the spatial dependence of a
270 variable; this can be represented by a semivariogram, i.e., the scatter diagram of
271 covariance with respect to spatial distance. The weighting of the running average is then
272 determined by the variogram model function, which is the fitted function to the
273 semivariogram (Burgess and Webster, 1980a). Theoretically, the covariance of spatial
274 data increases with distance and becomes a steady value at distances exceeding a
275 particular threshold (Burgess and Webster, 1980a,b; Kohsaka, 1998). This limited
276 distance is the range within which the data indicates spatial dependence. The spatial
277 dependencies of the data are also shown in the estimation variances, which provide a
278 measure of the uncertainty in the interpolation values. When directional anisotropy was
279 detected in semivariograms, geometric anisotropy was removed by applying an affine
280 transformation to the distances of the sample sites.

281 Spatial distributions of deposition thickness and mean grain-size data were
282 interpolated across the entire surveyed region. Semivariograms were calculated from the
283 measured data, and variogram models were fitted using the weighted least-squares
284 method. Both the interpolated values and estimation standard errors were shown as
285 color images.

286 4. Results

287 4.1 Topographic Features and Bedforms

288 In regions up to approximately 500 m from the shoreline, erosion by the
289 tsunami dominated where flute-like depressions with erosional fringes were observed

290 (Fig. 4C), ranging in diameter from 10 cm to several meters. Deformed sedimentary
291 features or upward injection of sands that are generally associated with liquefaction
292 were not observed. Although detailed topographic measurements were not conducted,
293 the severe erosion that removed the pine forest on the spit appeared to extend to a depth
294 of around 0.5 to 1 m. Analysis of aerial photographs (Fig. 3) indicated that the region
295 eroded by the tsunami was approximately $3.5 \times 10^5 \text{ m}^2$.

296 All power poles observed in Rikuzentakata City were bent by tsunami
297 inundation flows (Fig.4B), and the orientation of the fallen poles indicated that the
298 flooding direction was mostly northward within the main city area, whereas several
299 poles in the main city also indicate southward backwash currents (Fig. 7).

300 Tsunami deposits were distributed across the entire inundated area of
301 Rikuzentakata City (Figs. 5 and 6). In most areas, a uniform thickness generally draped
302 the natural topography. However, dunes were occasionally formed by flooding or
303 backwash currents in both the main city and the Otomo areas (Fig. 5A). Dunes are
304 composed of coarse sand and pebbles, with wavelengths generally ranging from 1 to 10
305 m. The largest dune was composed of cobble-sized gravels and was observed in the
306 Otomo area (Fig. 5A); it had a wavelength of 10 m and was 30–40 cm high. Flow
307 directions suggested by dune crests and foresets were southwestward (N230°) in the
308 main city area, and southeastward (N144°) in the Otomo area.

309 4.2 Thickness Variation

310 The field survey and kriging interpolation helped determine the thickness of the
311 tsunami deposits in Rikuzentakata City (Fig. 8). The transported sediment started to be
312 laid down approximately 500 m from the shoreline, and attained a maximum thickness

313 (31.5 cm) within the next 100 m. The thickness of the deposits then gradually decreased
314 landward; however, local variations in sediment thickness were observed in relation to
315 topographic depressions or elevations. The tsunami deposits continued to the maximum
316 extent of inundation, where the thickness of muddy deposits ranged from 0.5 to 2 cm
317 (Fig. 8; Table 2).

318 As the tsunami deposits varied in thickness throughout Rikuzentakata City, the
319 total deposition was calculated by summing the interpolated distribution, giving an
320 estimate of $6.1 \times 10^5 \text{ m}^3$ transported material (standard error $1.5 \times 10^3 \text{ m}^3$).

321 4.3 Sedimentary Structures and Units

322 Based on observation of sedimentary structures in pits and trenches, it was
323 determined that the tsunami deposits in Rikuzentakata City were composed of one to
324 four sedimentary units, identified by distinctive sedimentary structures and grain-size
325 changes (Figs. 9, 10 and 11). Each sedimentary unit ranged from 1 to 10 cm in thickness,
326 and showed a flat, layer-like geometry (Figs. 6, 9, 10 and 11). Each unit typically
327 consisted of inverse-graded sand overlain by normally graded or gravelly sand (Fig. 9).
328 The normally graded sub-unit was generally thicker than the inverse-graded one. The
329 boundary between these two sub-units was often a sharp erosional surface, and
330 occasionally the inverse-graded sub-unit was truncated. A thin mud drape (<1 cm)
331 occurred on the top of the normally graded division (Fig. 9). Each unit commonly
332 showed parallel lamination and, less frequently, current ripple cross-lamination could be
333 observed (Fig. 9). The lowermost unit was generally the thickest and coarsest, and often
334 contained large clasts, such as pebbles or cobbles, within sands (Fig. 10). The upper
335 units showed upward thinning and fining, and large clasts were rare in these units.

336 Each unit in the deposit showed evidence that it was formed under a
337 unidirectional runup or backwash current of the tsunami wave (Fig. 11). Grain fabric
338 analysis indicated that the flow direction was constant within an inverse-graded to
339 graded unit and varied from runup to the backwash current at the boundary between
340 units (Fig. 12). The paleocurrent direction shown by cross-lamination and dunes is
341 consistent with the grain-fabric data (Figs. 10, 11 and 12).

342 The thickness and number of units in the deposits decreased landward, and the
343 sandy sub-unit finally disappeared near the edge of tsunami inundation (Fig. 10 and 11),
344 although mud drapes were continuous. Flow-parallel variations in the thickness and
345 sedimentary structures of units were examined at two transects, one is in the eastern
346 region of the main city area (Transect 1) and another is in the Otomo area (Transect 2)
347 (Fig. 11). In Transect 1, the tsunami deposit was composed of two inverse-graded to
348 normally graded units at the seaward end (Fig. 11). The lower unit was a 15-cm-thick
349 very coarse pebbly sand, and showed thinning and fining landward. The upper unit was
350 a 5-cm-thick medium sand, which pinched out within 500 m. In Transect 2, three units
351 occurred at the upstream end of the runup current (Fig. 11). Grain-fabric analysis and
352 cross-lamination suggest that the first and third units were formed by the southeastward
353 runup current (Fig. 12), and that the second unit was formed by the northwestward
354 backwash current. The first unit was thick and was the coarsest, containing shell
355 fragments at its top. This unit showed fining and thinning down current, but continued
356 until the downstream end. The second unit was also thick, but pinched out within
357 approximately 500 m. The third unit was relatively thin and showed fining and thinning
358 down current.

359 4.4 Spatial Variation in Grain Size and Critical Flow Velocity for Particle
360 Motion

361 Analysis of spatial variation in grain sizes indicated landward fining (Fig. 13;
362 Table 2). Since the granulometric properties of the tsunami deposits vary vertically, we
363 plotted data obtained from the lowermost, coarsest unit in each site (Fig. 13). The
364 interpolated data of mean grain-size reveal that the center of the main city area was
365 covered by sandy deposits (Fig. 13), whereas samples taken from the northern end of
366 the inundation area were composed of muddy sediments. Thus, sand-sized sediments
367 diminished before the limit of the inundation area. Kriging interpolation of spatial
368 variation of mean grain-size suggests that the muddy sediments were transported 2 km
369 further than the distribution limit of the sandy deposits (Fig. 13).

370 Analysis of the critical flow velocity of the largest particles revealed that the
371 first flood wave exceeded 2.4 m/s at minimum (Fig. 14). A total of 21 sites were
372 examined, where gravels occurred in the lowermost unit of the tsunami deposit; the
373 estimated critical flow velocity ranged from 0.9 to 2.4 m/s when the flow height was set
374 to 10 m. The critical flow velocity ranged from 0.9 to 2.7 m/s when the flow height was
375 set to the estimated maximum inundation height of 15 m. Higher critical flow velocity
376 (2.4 or 2.7 m/s) was detected in the middle of the inundation area, slowing towards the
377 margins (0.9 m/s; Fig. 14).

378 4.5 Ostracods

379 The ostracod assemblages were recovered from sediments deposited by the
380 tsunami in the main city and Otomo area (collected at Locs. 19, 60, 94, 95 and 96 of Fig.
381 2 on April 25; Fig. 15 and Table 1). A sample taken at Loc. 60 contained abundant

382 ostracod specimens, and was characterized by inner bay species, such as
383 *Bicornucythere bisanensis* (Fig. 15B-1), *Nipponocythere bicarinata* (Fig. 15B-2),
384 *Spinileberis quadriaculeata* (Fig. 15B-3), and *Cytheromorpha acupunctata* (Fig. 15B-4).
385 It also contained some rocky shore species (*Aurila corniculata*, *Xestoleberis hanaii*)
386 (Table 1). Some of the ostracod valves of the sample were well preserved (Figs. 15B)
387 and translucent. Moreover, the soft parts were preserved in one *B. bisanensis* specimen
388 (Fig. 15B-1). However, many of the ostracod valves were opaque and fragmented,
389 indicating that the ostracod assemblage in the sample was probably derived from a
390 thanatocoenosis on the seafloor. Thus, it was appropriate to use MAT to compare the
391 assemblage of the sample at Loc. 60 with Holocene ostracod thanatocoenoses such as
392 those obtained from around Japan.

393 By applying MAT, we determined that the ostracod assemblage in the sample
394 of Loc. 60 was most similar to that of sample OK 28 from Osaka Bay; which had been
395 collected from a water depth of 9 m (Fig. 15A).

396 5. Discussion

397 5.1 Use of the Tsunami Deposits in Rikuzentakata City for the Identification 398 of Older Events

399 This study revealed that the tsunami deposits in Rikuzentakata City generally
400 consisted of multiple units that represented a discrete runup or backwash flow, as
401 described in Section 5.3 (Figs. 10, 11 and 16). Thus, for example, two inundations
402 produced four units (two runup and two backwash). This feature of the tsunami deposit

403 is quite different from that on the Sendai Plain, where multiple units were not obvious
404 (Goto et al., 2011). This difference could be attributed to differences in the tsunami
405 hydrographs and local topography.

406 Each unit was characterized by initial inverse grading and successive normal
407 grading that correspond to the accelerating and decelerating stages of the runup or
408 backwash flow respectively (Fig. 16). Multiple units with inverse- to normal-grading
409 were also reported from the 2004 Indian Ocean Tsunami deposits in Thailand (Naruse et
410 al., 2010) and other coastal environments (e.g., Kon'no, 1961; Shi et al., 1995; Benson
411 et al., 1997; Dawson & Smith, 2000; Gelfenbaum & Jaffe, 2003; Moore et al., 2006;
412 Nanayama & Shigeno, 2006), suggesting the general applicability of this facies model
413 of the multiple-bedded terrestrial tsunami deposits described here. Each unit of
414 multilayered tsunami deposits have often been attributed to a discrete wave (e.g.,
415 Kon'no, 1961; Clague et al., 2000) or one set of runup/backwash currents of a tsunami
416 (e.g., Moore & Moore, 1984; Nishimura & Miyaji, 1995; Nanayama & Shigeno, 2006).
417 Sedimentary features within multiple-bedded tsunami deposits are often complicated
418 (e.g., Moore et al., 2006) and their formative processes have been interpreted to be a
419 consequence of the multiple waves of tsunamis (e.g., Fujiwara, 2007). A characteristic
420 feature of tsunamis is the turnover of unidirectional current due to long wave period
421 (several minutes to tens of minutes) that involves acceleration, deceleration and
422 turnover stages.

423 The runup units are generally thicker than the backwash units probably because
424 of the asymmetric behavior of tsunami waves and the availability of source sediments
425 (Naruse et al., 2010). The tsunami waves run up with relatively uniform flow directions,
426 whereas those of the backwash currents are generally concentrated and localized

427 (Umitsu, 2006; Dodd et al., 2008). This asymmetric behavior of tsunami waves is
428 commonly observed in various environments (Umitsu, 2006; Naruse et al., 2010), and
429 can explain the fact that backwash units in the onshore tsunami deposit are often absent
430 or distributed only locally.

431 The importance of understanding the internal subunits of each unit in a tsunami
432 deposits is critical for the identification of the runup unit. Naruse et al. (2010) proposed
433 a facies model of tsunami deposits in which the basal inverse graded divisions (subunit
434 I) are produced during the waxing stage of the tsunami runup or backwash flows but
435 they are easily lost due to subsequent erosion (Fig. 16). An internal erosion surface
436 (IES) often develops between the inverse and normal graded subunits. As a result,
437 tsunami deposits are generally composed of graded units (subunit G) that are deposited
438 in the waning stage of flow and therefore have a greater preservation potential. In the
439 case of the runup flow, the stagnant stage of the tsunami wave forms silty mud drapes
440 (subunit S). Thus, it was suggested that the sequence ideally containing units I-G-S
441 corresponds to the runup flow and the sequence containing units I-G corresponds to the
442 backwash flow although there are large variations due to local erosion and deposition
443 (Fig. 16). The model assumes that deposition and erosion by tsunami waves are mostly
444 caused by spatial differences in the rate of sediment transport, and the sites of
445 deposition and erosion show a patchy distribution when the flow velocity field is
446 remarkably non-uniform. Thus, remarkable lateral variations in sedimentary structures
447 in a tsunami deposit can mostly be explained by localized erosional and depositional
448 processes.

449 Without this subunit I-G-S model (Naruse et al., 2010), the flow units in a
450 tsunami deposit may be misinterpreted. For example, the tsunami deposit in Loc. 93

451 appeared to be composed of 5–6 subunits that were bounded by mud drapes or erosional
452 surfaces (Fig. 16), but the grain-fabric analysis suggested that the deposit actually
453 consisted of three flow-units (2 runup and 1 backwash units) (Fig. 11 and 12). Erosional
454 surfaces are intercalated within a flow unit due to the waxing of the runup or backwash
455 flow, and the true unit boundaries are between the normal- and inverse-graded subunits
456 (subunits G to I) or silty mud drapes (subunit S).

457 The trends of landward fining and thinning of each unit and a decrease in the
458 number of units are also common features in various terrestrial environments (e.g.,
459 Fujino et al., 2010). The landward fining trend of each unit that differentiates the run-up
460 limit of the sandy and muddy sediments is an especially significant feature for
461 reconstructing inundation areas based on the distribution of ancient tsunami deposits.
462 Sandy tsunami deposits were distributed widely in the main city area, whereas muddy
463 deposits ($<4\ \phi$ on average) occurred near the margins of the inundation area (Fig. 13).
464 Kriging interpolation of the mean grain-size of the deposits revealed that the tsunami
465 can extend more than 2 km from the run-up limit of the sandy deposits (Fig. 13).
466 Therefore, it is suggested that precise reconstruction of tsunami inundation from
467 geological record requires the identification of muddy tsunami deposits (Goto et al.,
468 2011). While these may be quite difficult to distinguish from surrounding soils,
469 Chagué-Goff et al. (in press this issue) show that geochemical markers can successfully
470 differentiate between fine grained sediments of marine or terrestrial origin. It should
471 also be noted that the number of data control points is small in the northern region of the
472 study area so that the result of the Kriging method is similar to that of linear
473 interpolation. Thus, future analysis with a larger number of data control points is needed
474 to confirm the actual transition point between sandy and muddy tsunami deposits. In our

475 area, the number of internal sedimentary units also decreased landward as a result of
476 landward thinning of each unit. It is therefore recommended that the seaward end of a
477 tsunami deposit should be studied when attempting to estimate the number of waves
478 associated with inundation.

479 5.2 Reconstruction of Behavior of the Tohoku-Oki tsunami in Rikuzentakata 480 City

481 The behavior of the Tohoku-Oki tsunami in Rikuzentakata City reconstructed
482 from the analysis of tsunami deposits reveals that at least two waves inundated the city
483 with velocities exceeding 2.4 m/s. This estimation provides minimum value of the flow
484 velocity, and future study with evidence such as video footage or eye-witness accounts
485 will reveal the merits and limitations of this analysis of the wave properties from the
486 sediments. The analysis of the sediment flux and micropaleontological evidence
487 suggests that erosion of the seafloor of Hirota Bay may have occurred and the resulting
488 sediments probably transported on land.

489 In Transects 1 and 2, the basal, flooding flow, unit could be traced to the
490 landward end of both transects (Fig. 11). The first backwash flow unit occurred in the
491 seaward half of Transects 2, and pinched out near its center. The second runup flow unit
492 was also continuous in Transect 2, whereas it was no longer visible in the center of
493 Transect 1. Although the correlation between the sedimentary units in the main city area
494 was difficult due to the complexity of sedimentary units, a maximum of four runup units
495 could be recognized, suggesting that two or more waves also inundated this region. As
496 described above, data from a GPS buoy located approximately 15 km offshore indicates
497 that seven successive waves hit this coast (Takahashi et al., 2011), and that the first

498 wave was the largest. The first runup flow unit of the tsunami deposit in Rikuzentakata
499 City is the thickest, and therefore, it is reasonable to suggest that this unit may be
500 correlated with the first inundating wave. With regard to successive waves, it is difficult
501 to correlate these with flow units. Records from the GPS buoy indicate that the second
502 and fourth waves were relatively high (approximately 2 m in height), whereas others
503 were relatively small (less than 1.5 m in height). Hence, we tentatively correlate the
504 second flooding flow unit to the second or the fourth wave, although future
505 investigation using methods such as numerical simulation would seem necessary to
506 confirm this correlation.

507 The analysis of sediment flux implies that the tsunami deposit in Rikuzentakata
508 City included material not only from terrestrial erosion but also subaqueous erosion in
509 Hirota Bay. The paleontological evidence clearly indicates that the sediment source of
510 the tsunami deposit was at least partially from Hirota Bay. Bathymetric data indicate a
511 water depth of 9 m. The total amount of sediment deposited on land was estimated to be
512 $6.1 \times 10^5 \text{ m}^3$ (standard error: $1.5 \times 10^3 \text{ m}^3$). If all sediments were provided from the
513 sandy spit eroded by the first tsunami wave ($3.5 \times 10^5 \text{ m}^2$), the average depth of
514 erosional truncation would be approximately 1.7 m. Although the exact values should
515 be determined by a future survey, this depth of erosion seems unlikely on the basis of
516 visual observations. We infer that the erosional depth on the beach was less than 1 m
517 (Fig. 4C and 4D), and that nearly half of the sediments were transported from the
518 seafloor of Hirota Bay or from further offshore. Indeed, muddy sediments were widely
519 distributed near the landward end of the inundation area, suggesting another sediment
520 source of fine-grained sediments was available. Muddy sediments can be also sourced
521 from the rice paddy fields, but erosion in the study area was limited to the coastal area

522 where rice fields were not present (Fig. 3). Trench examination suggested that the rice
523 paddy fields were not markedly eroded (e.g. Fig. 6a), indicating a likely marine source
524 for the fine-grained tsunami deposits.

525

526 6. Conclusion

527 The 2011 Tohoku-Oki tsunami deposited a large amount of sediments on land.
528 A field survey at Rikuzentakata City, northeastern Japan, provided tsunami inundation
529 characteristics for this region and a facies model of deposition on the bay-head deltas of
530 estuarine systems.

531 (1) The tsunami deposit in Rikuzentakata City generally consisted of one- to
532 four units that represent a discrete runup or backwash flow. Each unit was characterized
533 by initial inverse grading (subunit I) and successive normal grading (subunit G), which
534 correspond to the accelerating and decelerating stages of the flow, respectively. Between
535 subunit I and G, an internal erosion surface often developed in response to the stage in
536 which the flow reached maximum shear velocity, truncating the underlying
537 inverse-graded subunit I. In case of the runup flow unit, the silty, fine-grained drapes
538 (subunit S) overlaid the graded interval (subunit G). Features of multiple units with
539 inverse-to-normal graded divisions are similar to the facies model for tsunami deposits
540 in coastal plains, suggesting the general applicability of the model to multiple-bedded,
541 terrestrial tsunami deposits.

542 (2) Correlation between the sedimentary structures and analysis of the grain
543 fabric of the tsunami deposit revealed that the Tohoku-Oki tsunami inundated

544 Rikuzentakata City at least twice, and that flow velocity exceeded 2.4 m/s.
545 Paleontological analysis of the sediment provenance and kriging estimation of the total
546 volume of the tsunami deposits indicate that the sediments were derived not only from
547 the eroded beach sands but also from the seafloor of Hirota Bay or more pelagic
548 regions.

549 All the inferences obtained from the study of tsunami deposits in Rikuzentakata
550 City can be used to refine future studies such as the development of numerical models.
551 Although offshore tsunami hydrograph data are available, the complicated shape of
552 Sanriku Coast affected the wave height and periodicity near the coast. Therefore,
553 hydrodynamic numerical models of tsunamis are important for future disaster
554 prevention planning, and data from tsunami deposits (such as the number of waves and
555 minimum flow velocities of runup flows) provide important constraints for model
556 verification. The amount and sources of sediments transported by the tsunami are also
557 important factors for model verification. Morphodynamic models require sediment
558 entrainment functions of bedload and suspended load for the calculation of landform
559 developments, and numerous types of empirical functions have been proposed by
560 various methods (e.g., Garcia and Parker, 1991). The choice of sediment entrainment
561 functions should be tested by natural cases of complicated shorelines such as the
562 tsunami deposits in Rikuzentakata City.

563 Acknowledgments

564 This survey was conducted as part of the research of The 2011 Tohoku
565 Earthquake Tsunami Joint Survey Group (www.coastal.jp/tsunami2011). We gratefully

566 acknowledge their sincere contributions. We are grateful to Hitoshi Shibuya and Takuya
567 Matsuzaki for their help with field sampling and grain-size measurements at Kochi Core
568 Center. This study is dedicated to all those affected by the March 11, 2011 earthquake.
569

570 References

- 571 Abe, T., Goto, K., Sugawara, D., in press this issue Relationship between the maximum
572 extent of tsunami sand and the inundation limit of the 2011 Tohoku-Oki
573 tsunami on the Sendai Plain, Japan. *Sedimentary Geology*,
574 doi:10.1016/j.sedgeo.2012.05.004.
- 575 Asano, T., Matsumoto, C., Nagano, A., 2009. Functional Assessment on Coastal Forests
576 in Japan as Tsunami Barrier Facilities. *Journal of Hydraulic, Coastal and*
577 *Environmental Engineering (JSCE) B2-65*, 1311-1315. (in Japanese with
578 English abstract)
- 579 Benson, B.E., Grimm, K.A. & Clague, J.J. 1997. Tsunami deposits beneath tidal
580 marshes on northwestern Vancouver Island, British Columbia. *Quaternary*
581 *Research* 48, 192-204.
- 582 Brownlie, W.R., 1981. Prediction of flow depth and sediment discharge in open
583 channels. Report No. KH-R-43A, Keck Laboratory of Hydraulics and Water
584 Resources, California Institute of Technology, Pasadena, California.
- 585 Burgess, T.M., Webster, R., 1980a. Optimal interpolation and isarithmic mapping I. The
586 semi-variogram and punctual kriging. *European Journal of Soil Science* 31,
587 315–331.

- 588 Burgess, T.M., Webster, R., 1980b. Optimal interpolation and isarithmic mapping. II.
589 Block kriging. *European Journal of Soil Science* 31, 505–524.
- 590 Chagué-Goff, C., Andrew, A., Szczuciński, W., Goff, J., Nishimura, Y. in press this issue.
591 Geochemical signatures up to the maximum inundation of the 2011
592 Tohoku-oki tsunami - implications for the 869 AD Jōgan and other
593 palaeotsunamis. *Sedimentary Geology*. doi:[10.1016/j.sedgeo.2012.05.021](https://doi.org/10.1016/j.sedgeo.2012.05.021)
594
- 595 Chida, N., Matsumoto, H., Obara, S., 1984. Recent Alluvial Deposit and Holocene Sea
596 level Change on Rikuzentakata Coastal Plain, Northeast Japan. *Tohoku-Chiri*
597 36, 232-239. (in Japanese with English abstract).
598
- 599 Clague, J.J., Bobrowsky, P.T., Hutchinson, I., 2000. A review of geological records of
600 large tsunamis at Vancouver Island, British Columbia, and implications for
601 hazard. *Quaternary Science Reviews* 19, 849-863.
- 602 Dawson, S., Smith, D.E., 2000. The sedimentology of Middle Holocene tsunami facies
603 in northern Sutherland, Scotland, UK. *Marine Geology* 170, 69-79.
- 604 Dodd, N., Stoker, A.M., Calvete, D., Sriariyawat, A., 2008. On beach cusp formation.
605 *Journal of Fluid Mechanics* 597, 145-169.
- 606 Einstein, H.A., 1950. The Bedload Function for Bedload Transportation in Open
607 Channel Flows. Technical Bulletin No. 1026 , U.S.D.A., Soil Conservation
608 Service, 1–71.
- 609 Folk, R.L., 1966. A review of grain-size parameters. *Sedimentology* 6, 344–359.
- 610 Fujii, Y., Satake, K., Sakai, S., Shinohara, M., Kanazawa, T., 2011. Tsunami source of
611 the 2011 off the Pacific coast of Tohoku Earthquake. *Earth Planets Space* 63,

612 815–820.

613 Fujino, S., Naruse, H., Matsumoto, D., Sakakura, N., Suphawajruksakul, A.,
614 Jarupongsakul, T., 2010. Detailed measurements of thickness and grain size
615 of a widespread onshore tsunami deposit in Phang-nga Province,
616 southwestern Thailand. *Island Arc* 19, 389–398.

617 Fujiwara, O., 2007. Major contribution of tsunami deposit studies to Quaternary
618 Research. *The Quaternary Research (Daiyonki kenkyu)* 46, 293–302.

619 Garcia, M.H., 2008. Sediment Transport and Morphodynamics. In: Garcia M.H. (Eds.),
620 Sedimentation engineering: processes, management, modeling, and practice.
621 American Society of Civil Engineers, Virginia, USA, pp. 21-163.

622 García, M.H., Parker, G., 1991. Entrainment of Bed Sediment into Suspension. *Journal*
623 *of Hydraulic Engineering, ASCE* 117, 414–435.

624 Gelfenbaum, G., Jaffe, B., 2003. Erosion and sedimentation from the 17 July, 1998
625 Papua New Guinea Tsunami. *Pure and Applied Geophysics* 160, 1969-1999.

626 Goto, K., Chagué-Goff, C., Fujino, S., Goff, J., Jaffe, B., Nishimura, Y., Richmond, B.,
627 Sugawara, D., Szczuciński, W., Tappin, D.R., Witter, R., Yulianto, E., 2011.
628 New insights of tsunami hazard from the 2011 Tohoku-oki event. *Marine*
629 *Geology* 290, 46-50.

630 Goto, K., Chagué-Goff, C., Goff, J., Jaffe, B. (submitted this issue). The future of
631 tsunami research following the 2011 Tohoku-oki event. *Sedimentary*
632 *Geology*

633 Harrington, R.F., 1967. *Field Computation by Moment Methods*, 1st ed. The Macmillan
634 Co., New York.

635 Hiscott, R.N., 1994. Loss of capacity, not competence, as the fundamental process

- 636 governing deposition from turbidity currents. *Journal of Sedimentary*
637 *Research* 64, 209-214.
- 638 Ikeya, N., Cronin, T.M., 1993. Quantitative analysis of Ostracoda and water masses
639 around Japan: application to Pliocene and Pleistocene paleoceanography.
640 *Micropaleontology* 39, 263-281.
- 641 Keulegan, G.H., 1938. Laws of turbulent flow in open channels. *Journal National*
642 *Bureau of Standards, Research Paper* 1151, 707–741.
- 643 Kohsaka, H., 1998. Kriging and its Geographic Applications. *Bulletin of Nihon*
644 *University College of Humanities and Sciences* 34, 27–35.
- 645 Kon’no, E., 1961. Geological observations of the Sanriku coastal region damaged by
646 Tsunami due to the Chile Earthquake in 1960. *Contributions from the*
647 *Institute of Geology and Paleontology, Tohoku University* 52, 1-40. (in
648 Japanese with English abstract)
- 649 Moore, J.G., Moore, G.W., 1984. Deposit from a giant wave on the island of Lanai,
650 Hawaii. *Science* 226, 1312–1315.
- 651 Moore, A., Nishimura, Y., Gelfenbaum, G., Kamataki, T., Triyono, R., 2006.
652 Sedimentary deposits of the 26 December 2004 tsunami on the northwest
653 coast of Aceh, Indonesia. *Earth, Planets and Space* 58, 253–258.
- 654 Mori, N., Takahashi, T., Yasuda, T., Yanagisawa, H., 2011. Survey of 2011 Tohoku
655 earthquake tsunami inundation and run-up, *Geophysical Research Letters* 38,
656 doi:10.1029/2011GL049210.
- 657 Nanayama F., Shigeno, K., 2006. Inflow and outflow facies from the 1993 tsunami in
658 southwest Hokkaido. *Sedimentary Geology* 187, 139–158.
- 659 Nanayama, F., Satake, K., Furukawa, R., Shimokawa, K., Atwater, B.F., Shigeno, K. &

660 Yamaki, S., 2003. Unusually large earthquakes inferred from tsunami
661 deposits along the Kuril trench. *Nature* 424, 660–663.

662 Naruse, H., Fujino, S., Suphawajruksakul, A., Jarupongsakul, T., 2010. Features and
663 formation processes of multiple deposition layers from the 2004 Indian
664 Ocean Tsunami at Ban Nam Kem, southern Thailand. *Island Arc* 19,
665 399–411.

666 National Police Agency of Japan, 2012. [http://www.npa.go.jp/archive/keibi/biki/
667 higaijokyo_e.pdf](http://www.npa.go.jp/archive/keibi/biki/higaijokyo_e.pdf).

668 Neill, C.R., Yalin. M.S., 1969. Qualitative definition of beginning of bed movement.
669 *Journal of the Hydraulics Division, ASCE* 95, 585–587.

670 Nelson, A.R., Sawai, Y., Jennings, A.E., Bradley, L.A., Gerson, L., Sherrod, B.L.,
671 Sabeau, J., Horton, B.P., 2008. Great-earthquake paleogeodesy and tsunamis
672 of the past 2000 years at Alsea Bay, central Oregon coast, USA. *Quaternary
673 Science Reviews* 27, 747–768.

674 Nettles, M., Ekstrom, G., Koss, H.C., 2011. Centroid-moment-tensor analysis of the
675 2011 off the Pacific coast of Tohoku Earthquake and its larger foreshocks
676 and aftershocks. *Earth, Planets and Space*, 63, 519–523.

677 Nishimura, Y., Miyaji, N., 1995. Tsunami deposits from the 1993 southwest Hokkaido
678 earthquake and the 1640 Hokkaido Komagatake eruption, northern Japan.
679 *Pure and Applied Geophysics* 144, 719–733.

680 Parker, G., 2005. ID morphodynamics of rivers and turbidity currents.
681 <http://cee.uiuc.edu/people/parkerg/morphodynamics_e-book.htm>.

682 Ramette, M.M., Heuzel, M.M., 1962. A study of pebble movement in the Rhone by
683 means of tracers. *La Houille Blanche, Special A.*, 389-398.

- 684 Shi, S., Dawson, A.G., Smith, D.E., 1995. Coastal sedimentation associated with the
685 December 12th 1992 Tsunami in Flores, Indonesia. *Pure and Applied*
686 *Geophysics* 144, 525–536.
- 687 Sperazza, M., Moore J.N., Hendrix M.S., 2004, High-Resolution Particle Size Analysis
688 of Naturally Occurring Very Fine-Grained Sediment Through Laser
689 Diffractometry. *Journal of Sedimentary Research* 74, 736-743.
- 690 Stimpson, I., 2011. Japan's Tohoku Earthquake and Tsunami. *Geology Today* 27, 96-98.
- 691 Switzer, A.D., Jones, B.G., 2008. Large-scale washover sedimentation in a freshwater
692 lagoon from the southeast Australian coast: sea-level change, tsunami or
693 exceptionally large storm? *The Holocene* 18, 787-803.
- 694 Takahashi, S., Toda, K., Kikuchi, Y., et al., 2011. Urgent Survey for 2011 Great East
695 Japan Earthquake and tsunami disaster in ports and coasts. Technical Note
696 of the Port and Airport Research Institute 1231, Port and Airport Research
697 Institute, Japan, Yokosuka, pp. 1-200.
- 698 Umitsu, M., 2006. Spatial distribution of tsunami flow and deposits of tsunami on the
699 Nam Khem Plain, southern Thailand. *Chikyu Monthly* 28, 546–552. (in
700 Japanese).
- 701 Van Rijn, L.C., 1982. Equivalent roughness of alluvial bed. *Journal of the Hydraulic*
702 *Division, ASCE* 108, 1215–1218.
- 703

Figure captions

704

705 Figure 1. Index maps of study area. A: Map of northeastern Japan showing epicenter of
706 Tohoku Oki earthquake. B: Study area.

707 Figure 2. Locality maps of the study area. Estimation of inundation area is based on the
708 Maps of the Area hit by the Tsunami of 11 March 2011, Northeast Japan by
709 Tsunami Damage Mapping Team, Association of Japanese Geographers
710 (http://danso.env.nagoya-u.ac.jp/20110311/map/index_e.html).

711 Figure 3. Airphotos of Rikuzentakata City provided by Geospatial Information
712 Authority of Japan. A: Airphoto taken before the tsunami (2010). White
713 arrows indicate Takata-Matsubara pine forest located on a wave-dominated
714 spit. B: Airphoto taken after the tsunami (March 13th 2011). Yellow dashed
715 lines indicate regions where erosional processes of the tsunami dominated.
716 The photo shows Takata-Matsubara was eroded by the tsunami.

717 Figure 4. Photographs taken at Rikuzentakata City. A: Broken building in Rikuzentakata
718 City. B: Poles flattened by the tsunami runup flow. C: Flute-like erosional
719 features. Scale is 1 m. D: Collapsed coastal levee and Takata-Matsubara pine
720 forest.

721 Figure 5. Photographs showing features of the tsunami deposit at Rikuzentakata City. A:
722 Dunes formed by backwash flow. B: Garbage accumulated at the maximum
723 extent of tsunami inundation area. C: Rice fields covered by tsunami deposits.
724 D: Tsunami deposits in the parking area (Loc. 111).

725 Figure 6. Pictures of flow-parallel vertical sections of tsunami deposits in Rikuzentakata

726 City. Left is the seaward direction in all pictures. A: Wall of trench excavated
727 at Loc. 31. Boundary between the tsunami deposit and the original surface of
728 the rice field is smooth and shows no erosional feature. B: Tsunami deposit
729 peeled off from a trench wall onto cloth using polyurethane resin at Loc 14.
730 Scale bar is 5 cm. C: Tsunami deposit peeled off from a trench wall at Loc 93.
731 Cross lamination shows that the middle part of this deposit was formed by
732 backwash flow. Scale bar is 10 cm.

733 Figure 7. Directions of tsunami inundation flow measured from damaged artificial
734 objects such as bent power poles. Runup currents are dominant.

735 Figure 8. Thickness distributions of the tsunami deposit. A: Bubble plot of thickness of
736 the tsunami deposit at each sampling location. B: Kriging estimation of
737 spatial thickness distribution of the tsunami deposit in Rikuzentakata City.
738 White dashed line indicates distribution limit of sandy deposits. C: Standard
739 error of the result of the kriging estimation.

740 Figure 9. A typical example of the vertical variation of the tsunami deposit (Loc. 11E) in
741 mean grain-size. The deposit is characterized by inverse- to normal-graded
742 multiple units, although it lacks a silty subunit (subunit S). Bars indicate the
743 standard deviation of grain-size distribution at each interval.

744 Figure 10. Columnar sections showing cross profile of tsunami sand sheets in the main
745 city area of Rikuzentakata City. The locations of the sections are indicated in
746 Figure 2. The top of each columnar section corresponds to the local ground
747 surface. Reconstructions of paleo-flow directions are based on grain fabric
748 (Loc.19) and cross-laminations (Loc. 11W). Scale bars are 10 cm.

749 Figure 11 , Stratigraphic sections on flow-parallel transects showing a cross profile of

750 tsunami sand sheets in Otomo Area of Rikuzentakata City. The locations of
751 the two transects are indicated in Figure 2. The top of each section
752 corresponds to the local ground surface. Scale bars are 10 cm.

753 Figure 12. Rose diagrams showing results of grain fabric analysis of the tsunami deposit
754 in vertical sections. Imbrication angles of sand-sized grains at flow-parallel
755 vertical sections were examined and the runup and backwash flow units were
756 identified at each locality.

757 Figure 13. Mean grain-size distribution of the basal unit of the tsunami deposit. A:
758 Bubble plot of mean grain-size of the tsunami deposit at each sampling
759 location. B: Kriging estimation of spatial distribution of mean grain-size. C:
760 Standard error of the kriging estimation results.

761 Figure 14 Bubble plot of the critical flow velocity of gravels. The runup or backwash
762 flow of the tsunami in Rikuzentakata City must exceed these values at each
763 sampling point.

764 Figure 15. A: Map of Japan showing locations of the study area and the reference site
765 OK28. B: Scanning electron microscope images of characteristic species
766 recovered from sample c: (1) *Bicornucythere bisanensis* (2) *Nipponocythere*
767 *bicarinata*; (3) *Spinileberis quadriaculeata*; (4) *Cytheromorpha acupunctata*.

768

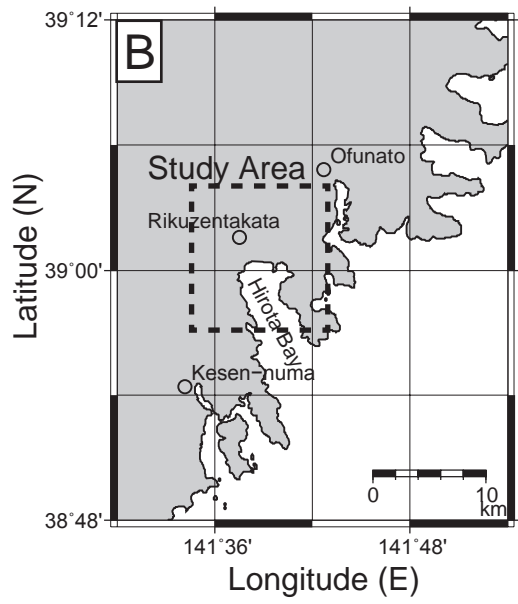
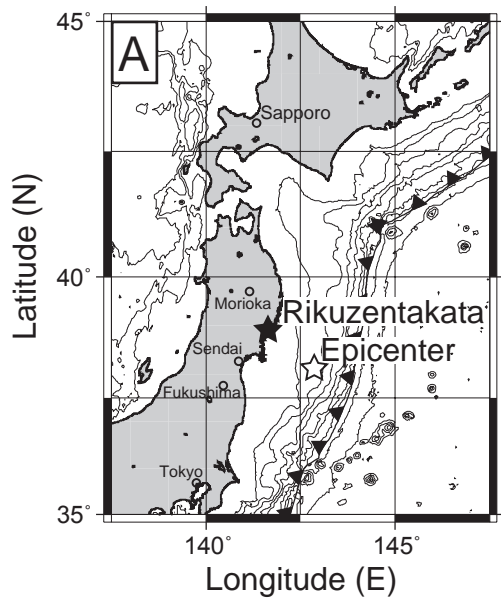
769 Figure 16 Schematic model of the formation process of multiple-bedded tsunami
770 deposits. A: Typical variation of the tsunami sequence that was frequently
771 observed in Rikuzentakata City. Subunits I, G and S indicate inverse-graded,
772 graded, and silty subunits. The ideal tsunami sequence formed by a single
773 wave is composed of two units, consisting of subunits I-G-S-I-G. At the

774 turnover stage from backwash to run-up, there is no ponding of stagnant
775 water on land so that a thick, silty subunit (subunit S) is not found at the top
776 of the backwash depositional unit. Inverse-graded subunits of runup flow
777 units and 1st backwash-flow unit were lost due to erosion. B: Schematic
778 formative process of the inverse- to normal-graded bedding in the tsunami
779 deposit. Flow conditions for processes 1-3 are shown in Figure 16A. An
780 internal erosion surfaces (IES) often develops between the inverse and normal
781 graded subunits.

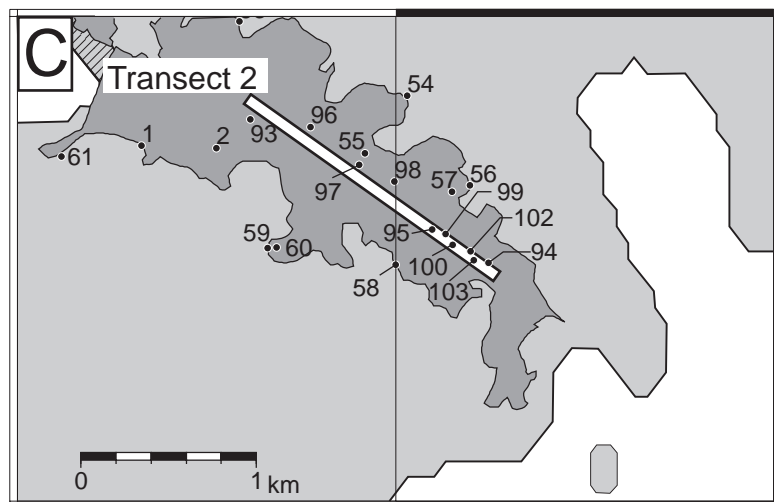
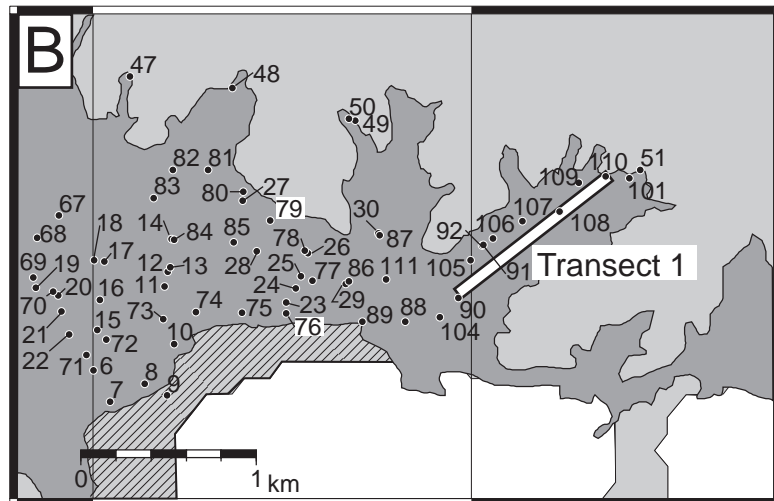
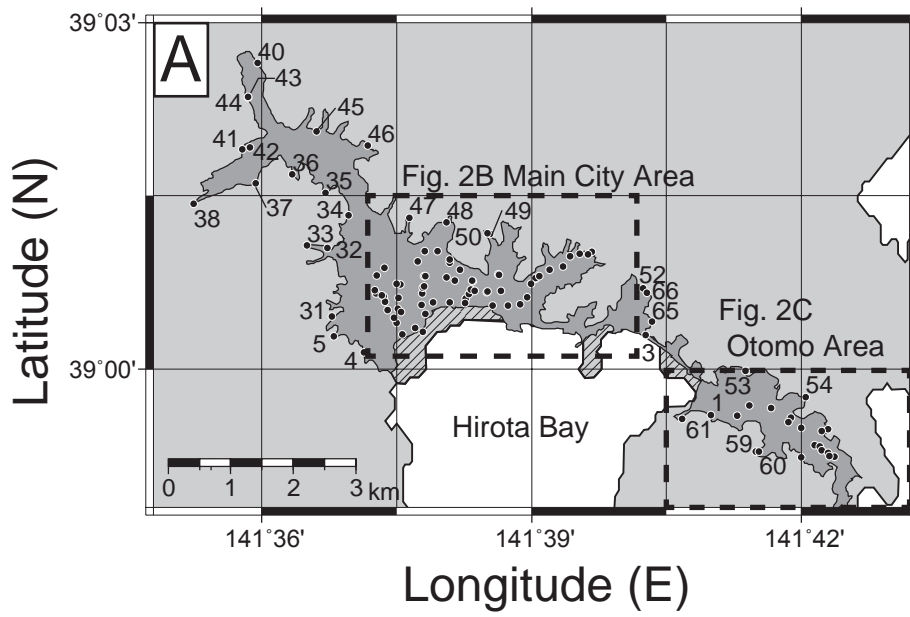
782

783 Table 1. Ostracods species observed in the tsunami deposits.

784 Table 2. Result of grain-size analysis by laser granulometer. All grain-size values are
785 shown in phi scale. Max. G is the maximum grain size.



Naruse et al. Fig. 1



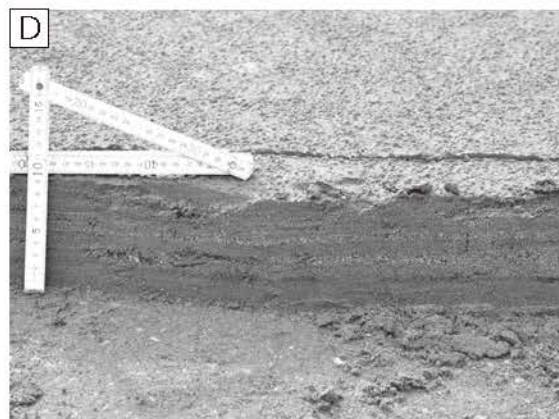
Inundation area
 Eroded area

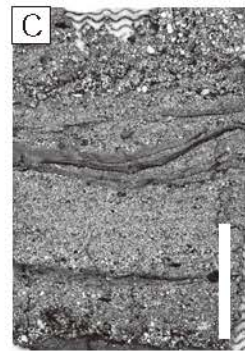
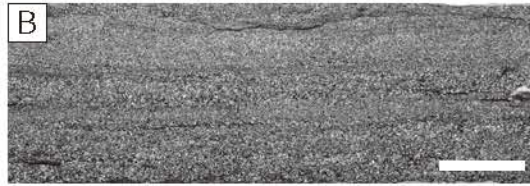
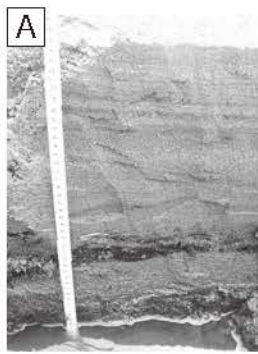
Naruse et al. Fig. 2

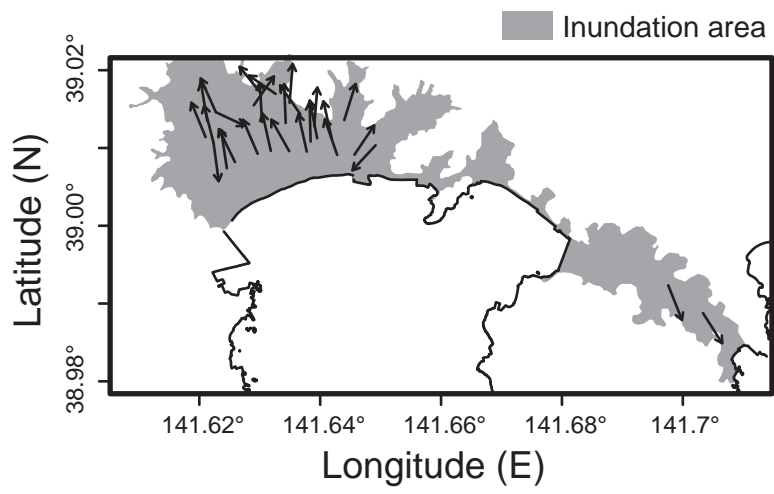


Naruse et al. Fig. 3



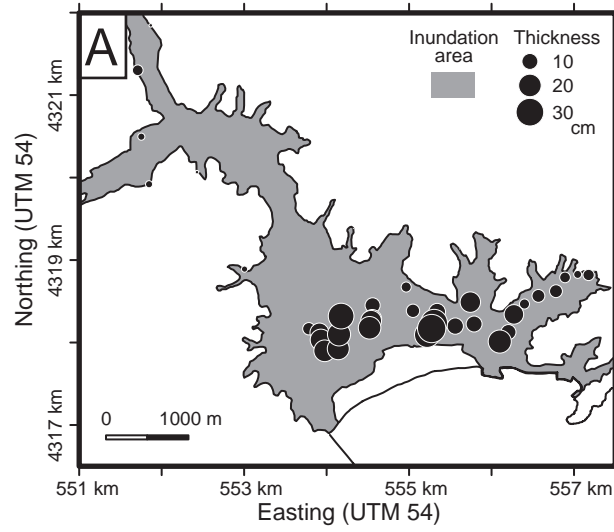




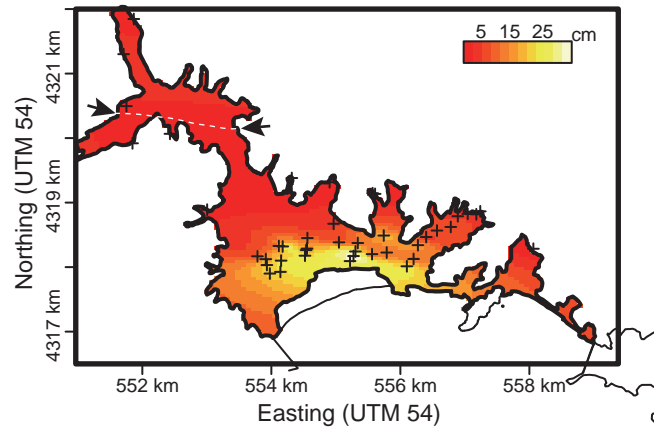


Naruse et al. Fig. 7

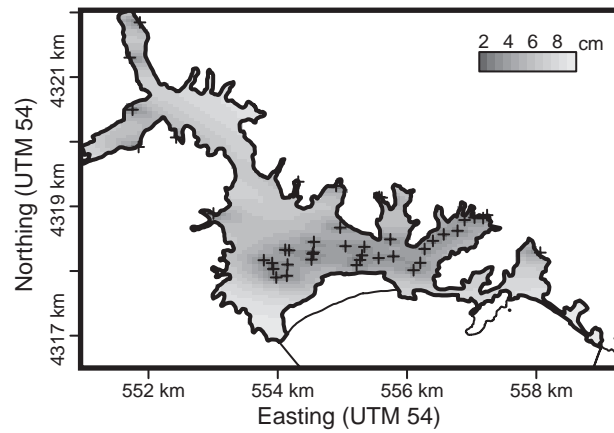
Thickness of tsunami deposit at each sampling point

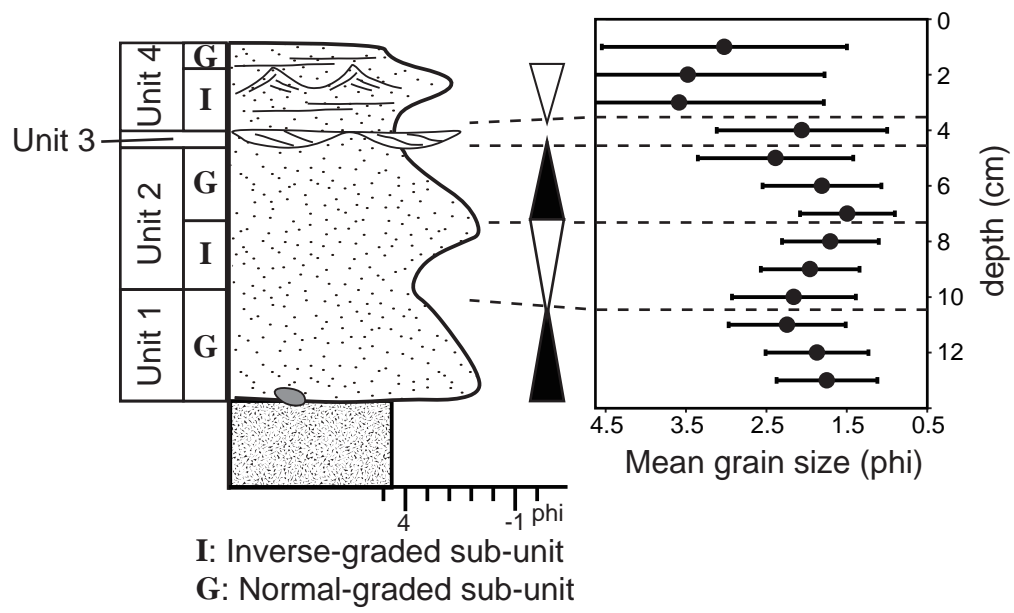


Estimated thickness distribution of tsunami deposit

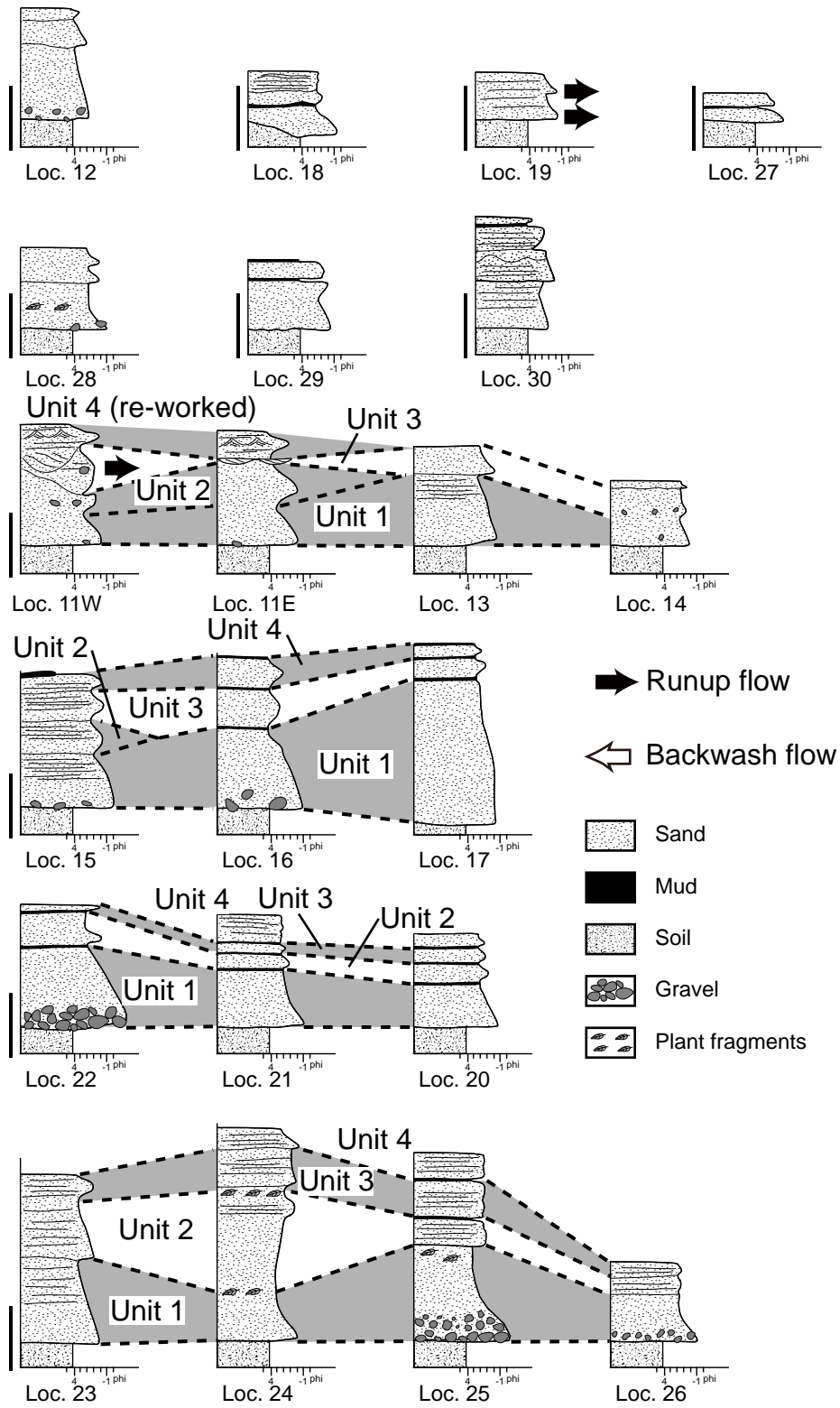


Standard error of thickness estimation

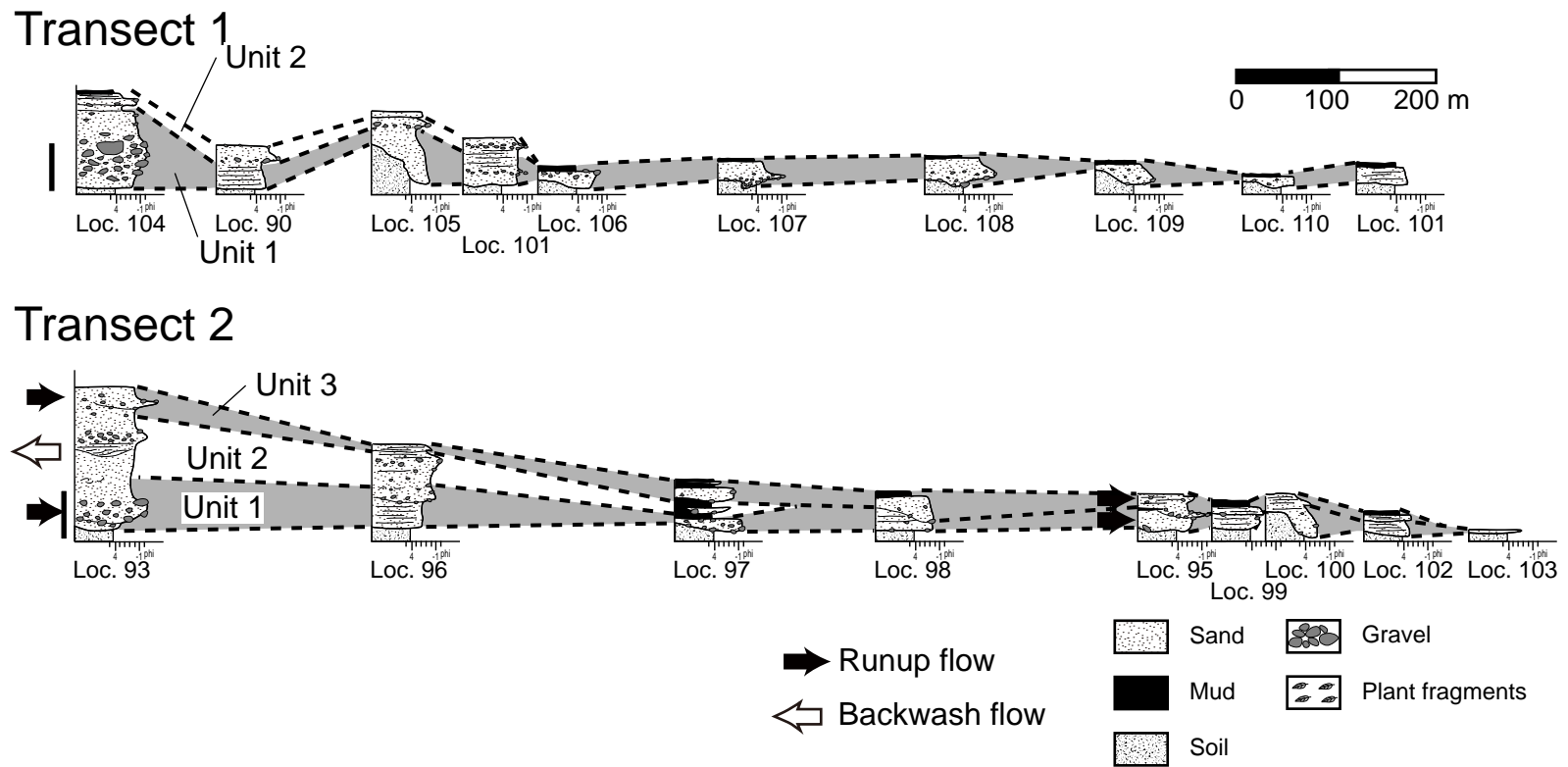




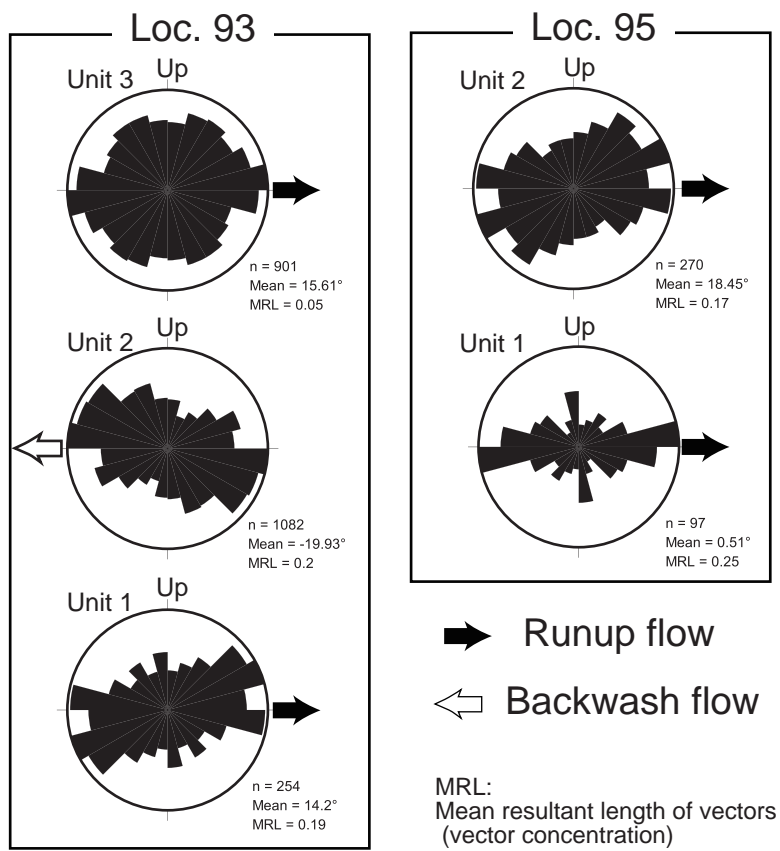
Naruse et al. Fig. 9



Naruse et al. Fig. 10

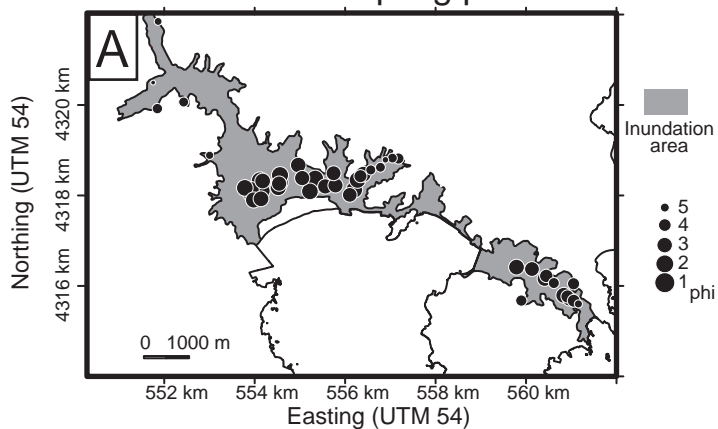


Naruse et al. Fig. 11.

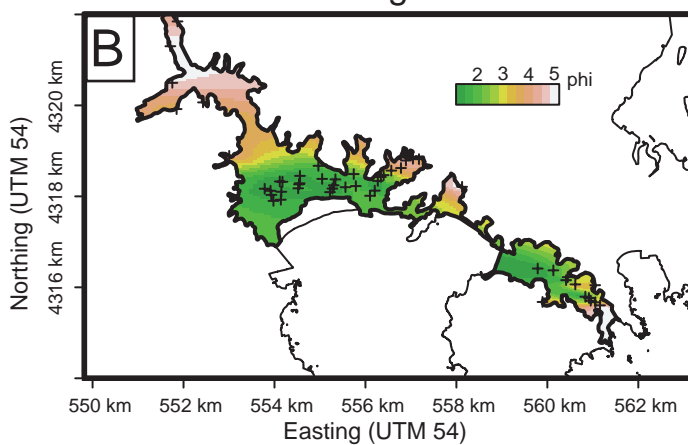


Naruse et al. Fig. 12

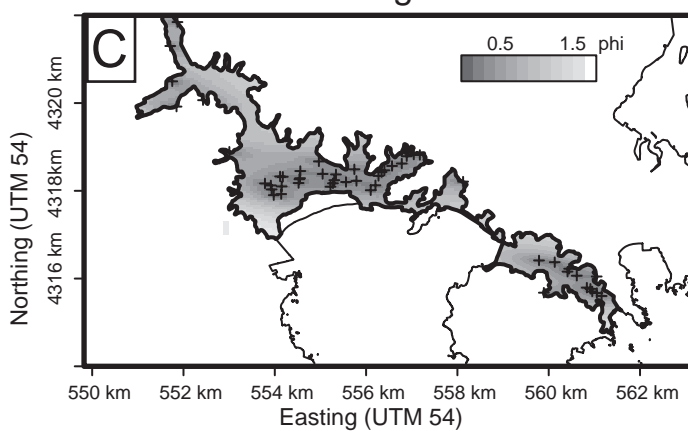
Mean grain size at each sampling point

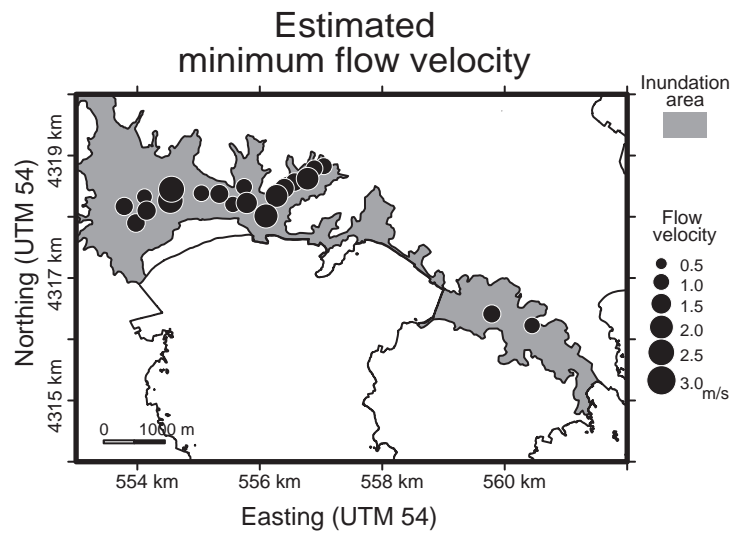


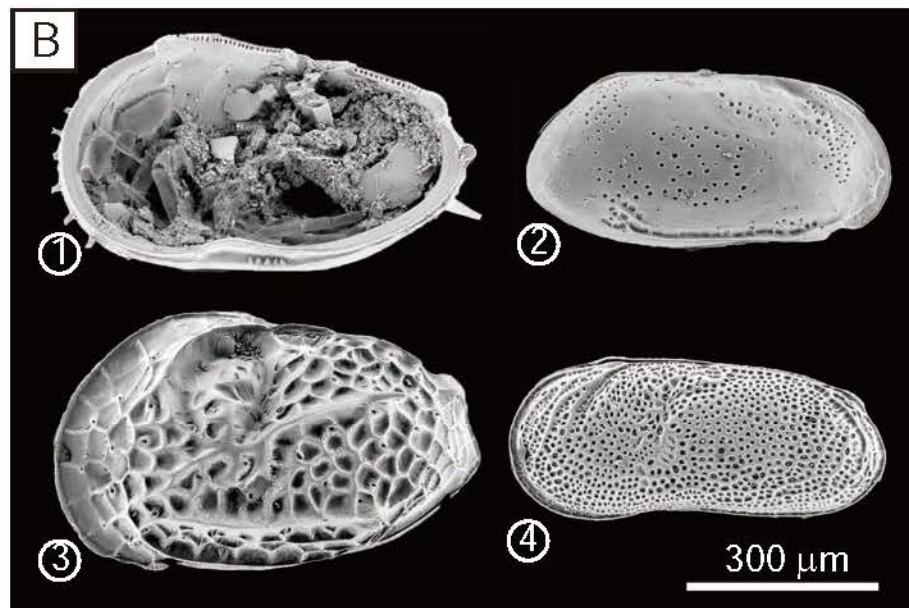
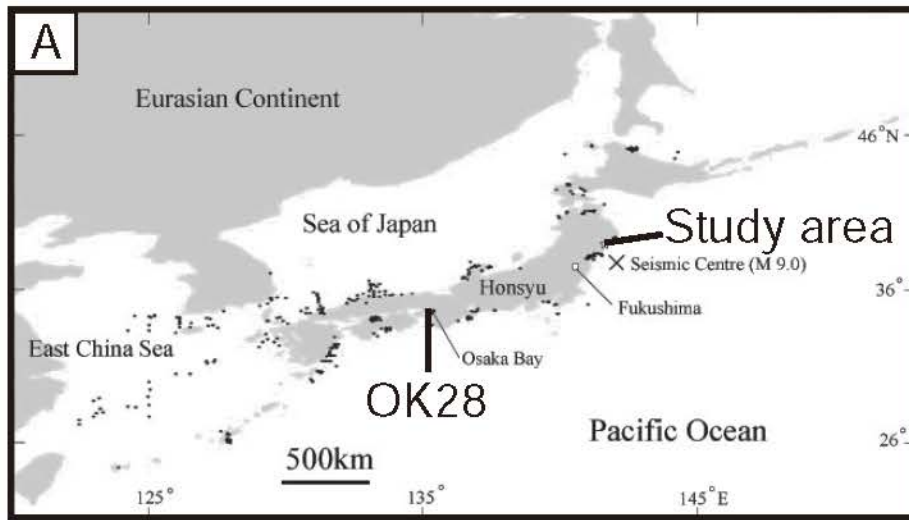
Estimated spatial distribution of mean grain size

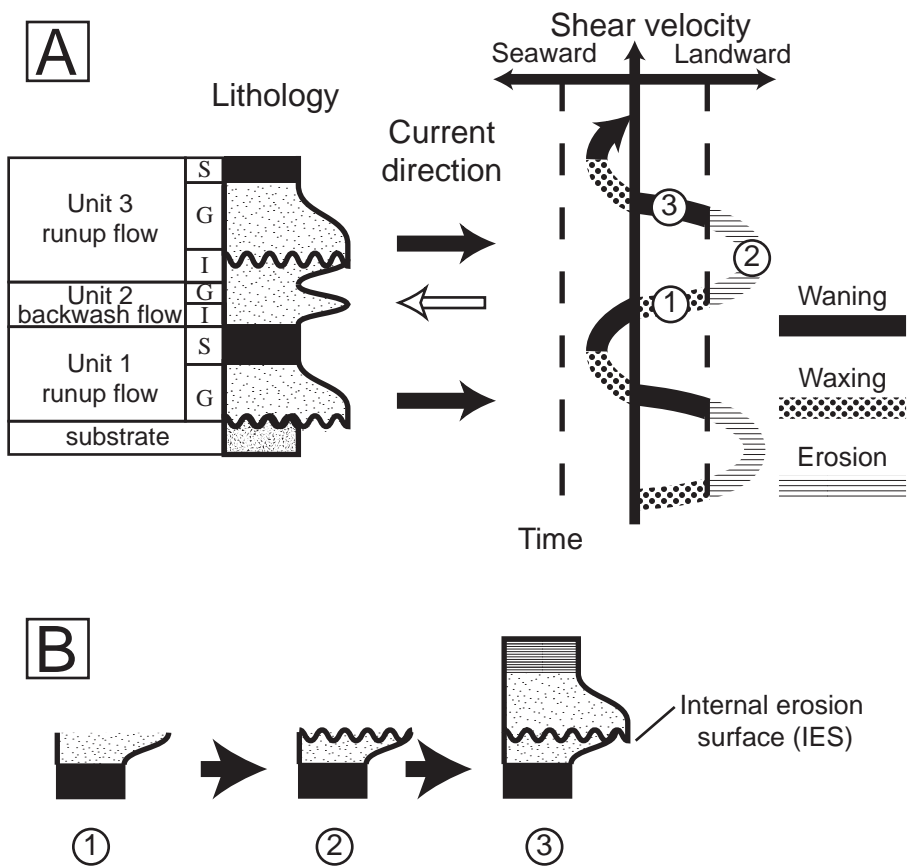


Standard error of estimation of mean grain size









	Loc.19	Loc.96	Loc. 60	Loc.94	Loc.95
<i>Ambtonia obai</i>			3	1	
<i>Angulicytherura miii</i>	1				
<i>Aurila corniculata</i>			14	11	
<i>Bicornucythere bisanensis</i>			36	17	
<i>Bythoceratina hanaii</i>			2		
<i>Bythoceratina hanaii</i>			2		
<i>Callistocythere japonica</i>			1		
<i>Callistocythere undulatifacialis</i>			2		
<i>Coquimba ishizakii</i>			3		
<i>Cornucoquimba tosaensis</i>			3		1
<i>Cytherois nakanoumiensis</i>			2		
<i>Cytheromorpha acupunctata</i>			6	3	
<i>Hemicytherura kajiyamai</i>			3	1	
<i>Howeina leptocytheroidea</i>			3	1	
<i>Kobayashiina donghaiensis</i>			2		
<i>Loxoconcha epeterseni</i>			1		1
<i>Loxoconcha japonica</i>			2		
<i>Loxoconcha ozawai</i>			2		
<i>Loxoconcha uranouchiensis</i>			3	1	
<i>Neonesidea oligodentata</i>			9	2	
<i>Nipponocythere bicarinata</i>			8	1	
<i>Parakrithella pseudadonta</i>			1		
<i>Pistocythereis bradyformis</i>			2		
<i>Pontocythere subjaponica</i>		1	6	2	4
<i>Schizocythere kishinouyei</i>				2	
<i>Semicytherura miurensis</i>			5		
<i>Spinileberis quadriaculeata</i>			16	16	
<i>Xestoleberis hanaii</i>			19	3	1
<i>Xestoleberis sagamiensis</i>			1		
<i>Xestoleberis setouchiensis</i>				2	
Total	1	1	157	63	7

Loc. No.		sand (%)	mud (%)	Mean	Sorting	Skewness	Kurtosis	D10	D50	D90	Max. G.
11	Total	92.8	7.2	2.27	0.95	0.66	3.96	3.56	2.15	1.16	
	Unit 1	99.6	0.4	1.99	0.68	0.37	3.49	2.87	1.97	1.12	
	Unit 2	92.4	7.6	2.17	0.96	0.70	4.15	3.45	2.06	1.04	
	Unit 4	76.7	23.3	3.25	1.61	1.28	4.56	5.64	2.89	1.60	
12	Total	98.4	1.6	1.96	0.79	1.31	7.79	2.84	1.90	1.04	
	Unit 1	98.7	1.3	2.10	0.74	1.02	6.27	2.96	2.06	1.21	-8.58
	Unit 2	97.7	2.3	1.58	0.94	2.09	11.98	2.51	1.48	0.57	
13	Total	97.6	2.4	1.69	0.93	1.82	10.08	2.66	1.59	0.68	
	Unit 1	98.0	2.0	1.66	0.89	1.63	9.42	2.65	1.57	0.67	
	Unit 2	96.5	3.5	1.75	1.04	2.28	11.73	2.70	1.62	0.70	
14	Total	96.4	3.6	1.65	0.89	1.01	6.43	2.77	1.55	0.64	
	Unit 1	100.0	0.0	1.41	0.61	0.13	2.40	2.24	1.40	0.60	-8.74
	Unit 2	97.8	2.2	1.59	0.92	2.14	12.67	2.52	1.50	0.61	
	Unit 3	78.2	21.8	2.80	1.88	1.16	3.87	5.66	2.28	0.90	
15	Total	92.6	7.4	1.98	1.17	1.91	9.52	3.24	1.80	0.79	
	Unit 1	93.5	6.5	2.20	1.15	2.29	11.20	3.33	2.01	1.09	
	Unit 2	87.8	12.2	2.34	1.24	0.99	4.60	4.01	2.15	0.95	
	Unit 3	95.6	4.4	1.72	1.07	2.08	11.43	2.84	1.57	0.60	
16	Unit 4	96.3	3.7	1.10	1.19	2.68	12.89	2.02	0.89	0.03	
	Total	96.5	3.5	1.73	1.00	2.28	12.26	2.68	1.60	0.72	
	Unit 1	97.4	2.6	1.37	0.98	2.49	13.63	2.25	1.23	0.41	-6.18
	Unit 2	93.8	6.2	2.53	1.09	1.79	8.74	3.63	2.39	1.37	
17	Unit 3	97.2	2.8	1.88	0.93	2.25	12.68	2.78	1.78	0.92	
	Total	87.3	12.7	2.12	1.63	1.82	6.37	4.47	1.67	0.68	
	Unit 1	87.9	12.1	1.91	1.69	1.86	6.26	4.41	1.42	0.47	
	Unit 2	91.6	8.4	2.71	1.18	2.00	8.78	3.81	2.52	1.55	
18	Unit 3	73.7	26.3	3.41	1.70	1.11	3.88	6.06	3.02	1.64	
	Total	96.8	3.2	1.66	0.97	1.53	8.38	2.63	1.57	0.62	
	Unit 1	96.3	3.7	1.25	1.09	2.96	15.07	2.02	1.09	0.30	-4.70
	Unit 2	100.0	0.0	1.37	0.62	0.19	2.49	2.21	1.35	0.56	
19	Unit 3	95.3	4.7	2.26	1.08	1.00	5.61	3.53	2.19	0.98	
	Total	99.0	1.0	1.46	0.76	1.09	6.92	2.35	1.39	0.58	
	Unit 1	97.9	2.1	1.54	0.91	2.01	11.41	2.49	1.43	0.57	-5.78
	Unit 2	100.0	0.0	1.38	0.61	0.17	2.44	2.21	1.36	0.58	
20	Total	97.8	2.2	1.68	0.93	1.47	7.92	2.67	1.57	0.69	
	Unit 1	96.4	3.6	1.45	1.12	2.22	10.73	2.53	1.26	0.36	
	Unit 2	100.0	0.0	2.08	0.62	0.13	2.43	2.92	2.07	1.26	
	Unit 3	100.0	0.0	1.89	0.66	0.10	2.44	2.78	1.88	1.01	
22	Unit 4	97.4	2.6	1.89	0.89	1.85	10.38	2.80	1.80	0.92	
	Total	90.0	10.0	1.94	1.24	1.94	10.22	3.45	1.72	0.68	
	Unit 1	95.1	4.9	1.61	1.15	2.17	11.64	2.94	1.40	0.50	-5.93
	Unit 2	69.8	30.2	3.27	1.63	1.03	4.54	5.49	3.01	1.43	
23	Total	99.7	0.3	1.56	0.68	0.37	3.54	2.44	1.53	0.69	
	Unit 1	100.0	0.0	1.53	0.66	0.14	2.43	2.42	1.51	0.65	
	Unit 2	100.0	0.0	1.53	0.63	0.11	2.42	2.38	1.51	0.69	
	Unit 3	97.3	2.7	1.80	0.92	2.04	11.34	2.71	1.70	0.82	
24	Total	97.8	2.2	1.96	0.84	1.50	8.52	2.83	1.88	1.03	
	Unit 2	97.1	2.9	2.01	0.92	1.92	10.40	2.88	1.91	1.06	
	Unit 3	98.8	1.2	1.96	0.74	0.95	5.88	2.84	1.92	1.06	
	Unit 4	99.5	0.5	1.71	0.66	0.53	4.39	2.56	1.69	0.87	
25	Total	96.7	3.3	1.68	1.00	1.55	7.75	2.57	1.55	0.68	
	Unit 1	94.8	5.2	1.55	1.25	2.32	10.40	2.52	1.34	0.41	
	Unit 2	98.6	1.4	1.97	0.71	1.31	7.90	2.76	1.93	1.14	
	Unit 3	100.0	0.0	1.82	0.60	0.09	2.37	2.62	1.81	1.03	
26	Unit 4	100.0	0.0	1.90	0.56	0.06	2.45	2.64	1.90	1.17	
	Total	96.3	3.7	1.59	1.09	2.35	11.77	2.53	1.43	0.54	
	Unit 1	95.8	4.2	1.49	1.14	2.54	12.30	2.43	1.31	0.44	-6.08
	Unit 2	98.0	2.0	1.92	0.90	1.68	9.93	2.89	1.84	0.90	
27	Total	94.4	5.6	1.98	1.20	1.94	9.19	3.15	1.81	0.78	
	Unit 1	91.8	8.2	1.97	1.39	1.87	7.43	3.33	1.71	0.63	
	Unit 2	97.0	3.0	2.00	1.02	2.01	10.95	2.97	1.90	0.92	
28	Total	97.1	2.9	2.19	0.84	1.07	6.21	3.16	2.11	1.23	
	Unit 1	99.7	0.3	2.11	0.63	0.48	4.46	2.91	2.09	1.30	-5.11
	Unit 2	94.5	5.5	2.28	1.05	1.67	7.96	3.41	2.13	1.16	
29	Total	97.9	2.1	1.88	0.87	1.44	8.28	2.80	1.81	0.90	
	Unit 1	99.0	1.0	2.08	0.73	0.83	5.71	2.95	2.06	1.19	-5.00
	Unit 2	97.7	2.3	1.61	0.95	1.91	11.03	2.57	1.52	0.58	
	Unit 3	95.9	4.1	1.69	1.12	2.28	11.21	2.66	1.53	0.59	

30	Total	97.0	3.0	2.04	0.94	1.82	10.09	3.01	1.94	1.01	-5.21
	Unit 1	96.7	3.3	2.23	0.96	1.69	9.17	3.24	2.13	1.18	
	Unit 2	97.6	2.4	1.85	0.90	1.90	10.94	2.77	1.76	0.86	
	Unit 3	96.7	3.3	2.03	0.98	1.90	10.20	3.02	1.92	0.99	
32		35.3	64.7	4.78	1.80	0.02	2.73	7.22	4.71	2.45	
36		59.3	40.7	3.93	1.91	0.59	2.78	6.81	3.52	1.82	
37		64.2	35.8	3.81	1.73	0.89	3.60	6.54	3.46	2.00	
40		53.1	46.9	4.23	2.07	0.35	2.50	7.33	3.84	1.82	
41		36.4	63.6	4.70	1.85	-0.03	2.76	7.18	4.64	2.43	
43		31.1	68.9	5.01	1.89	-0.11	2.42	7.49	5.08	2.51	
54		81.7	18.3	2.76	1.67	0.85	3.97	4.89	2.60	0.78	-5.09
56		75.6	24.4	3.16	1.90	1.06	3.55	6.24	2.70	1.17	
59		66.3	33.7	3.42	1.98	0.72	2.65	6.42	2.89	1.22	
66		30.6	69.4	4.96	1.98	-0.25	2.40	7.44	5.16	2.08	
90	Total	90.5	9.5	2.02	1.47	1.64	6.46	3.90	1.70	0.58	
	Unit 1	92.7	7.3	1.88	1.49	1.56	6.77	3.57	1.64	0.37	
	Unit 2	95.3	4.7	1.50	1.30	2.19	9.96	2.69	1.28	0.26	
91	Total	89.8	10.2	2.08	1.48	1.61	6.13	4.05	1.74	0.64	
	Unit 1	84.5	15.5	2.86	1.60	1.56	5.40	5.27	2.49	1.32	-5.61
	Unit 2	81.6	18.4	3.17	1.39	1.31	5.70	4.71	2.97	1.71	
93	Total	91.7	8.3	1.80	1.46	1.64	6.35	3.69	1.46	0.38	
	Unit 1	90.7	9.3	1.89	1.50	1.58	5.92	3.87	1.52	0.43	-5.73
	Unit 2	93.7	6.3	1.67	1.37	1.72	7.08	3.34	1.37	0.31	
	Unit 3	92.5	7.5	1.64	1.43	1.81	7.02	3.49	1.31	0.29	
94		53.1	46.9	4.18	1.75	0.58	2.79	6.78	3.86	2.16	
95		90.0	10.0	1.84	1.54	1.80	6.42	3.98	1.44	0.44	
96	Total	85.1	14.9	2.45	1.54	1.29	5.31	4.40	2.18	0.79	
	Unit 1	91.1	8.9	2.22	1.35	1.71	6.92	3.80	1.95	0.88	
	Unit 2	92.6	7.4	1.97	1.36	1.38	5.75	3.64	1.71	0.53	
97	Total	76.7	23.3	2.84	1.77	0.86	3.65	5.26	2.57	0.80	
	Unit 1	87.2	12.8	2.15	1.65	1.27	4.71	4.35	1.76	0.45	
	Unit 2	76.1	23.9	2.98	1.71	0.71	3.50	5.20	2.85	0.89	
98		64.1	35.9	3.48	2.07	0.60	2.55	6.58	3.11	1.06	
99	Total	68.6	31.4	3.29	1.83	0.81	3.21	5.98	2.90	1.25	
	Unit 1	78.6	21.4	2.77	1.74	1.07	3.73	5.37	2.32	0.94	
	Unit 2	58.5	41.5	3.73	1.82	0.49	2.59	6.28	3.53	1.50	
100	Total	67.6	32.4	3.36	1.86	0.79	3.17	6.12	2.95	1.30	
	Unit 1	80.3	19.7	2.72	1.71	1.19	4.07	5.29	2.27	0.98	
	Unit 2	65.1	34.9	3.61	1.82	0.75	2.90	6.33	3.21	1.56	
101		59.3	40.7	3.72	1.99	0.52	2.62	6.63	3.33	1.40	
102	Total	83.0	17.0	2.67	1.58	1.30	5.55	4.48	2.44	0.96	
	Unit 1	78.0	22.0	2.93	1.70	1.00	3.76	5.41	2.58	1.08	
	Unit 2	56.7	43.3	3.83	1.77	0.42	2.78	6.29	3.67	1.61	
104	Total	86.3	13.7	2.52	1.55	1.42	6.08	4.18	2.30	0.88	
	Unit 1	91.6	8.4	2.30	1.45	1.61	6.85	3.66	2.11	0.80	
	Unit 2	75.2	24.8	2.81	2.06	0.83	3.02	6.01	2.34	0.54	
	Unit 3	51.8	48.2	4.13	1.86	0.42	2.56	6.73	3.93	1.83	-8.05
105	Total	90.5	9.5	1.61	1.68	1.65	6.03	3.99	1.20	0.03	
	Unit 1	88.7	11.3	1.52	1.78	1.77	5.89	4.30	1.02	-0.04	-7.57
	Unit 2	95.5	4.5	1.65	1.40	1.48	6.78	3.15	1.46	0.14	
	Unit 3	90.8	9.2	2.00	1.60	1.29	5.32	3.84	1.78	0.25	
106	Total	78.5	21.5	2.43	1.91	1.27	4.34	5.39	1.91	0.54	
	Unit 1	86.6	13.4	1.86	1.89	1.56	5.01	4.84	1.28	0.15	-6.38
	Unit 2	54.0	46.0	4.13	1.99	0.42	2.36	7.05	3.78	1.71	
107		59.0	41.0	3.74	1.99	0.51	2.39	6.61	3.37	1.39	-5.95
108		55.8	44.2	3.78	2.41	0.30	1.88	7.18	3.40	0.84	-7.54
109		33.5	66.5	4.87	1.89	-0.09	2.36	7.33	4.95	2.24	-5.48
110		59.9	40.1	3.80	1.94	0.60	2.55	6.69	3.41	1.54	-5.32
111	Total	93.1	6.9	2.41	1.19	1.59	7.93	3.63	2.27	1.15	
	Unit 1	97.0	3.0	2.23	1.00	1.57	8.86	3.25	2.15	1.12	-7.01
	Unit 2	91.2	8.8	2.59	1.29	1.77	7.96	3.83	2.42	1.29	
	Unit 3	88.5	11.5	2.54	1.40	1.43	6.36	4.06	2.34	1.07	